AGU PUBLICATIONS

JGR

Journal of Geophysical Research: Space Physics

RESEARCH ARTICLE
10.1002/2016JA023793

Key Points:
- Data from one solar wind cycle are used to study the lagged (Pearson) correlation between solar wind parameters and geomagnetic indices
- The impact of solar wind structuring and magnetospheric inherent response time on the result is analyzed
- The solar wind structuring at the interface between fast/slow solar wind has strong impact on the results of the lagged correlation analysis

Supporting Information:
- Supporting Information S1

Correspondence to:
R. Maggiolo,
maggiolo@aeronomie.be

Citation:
Maggiolo, R., Hamrin, M., De Keyser, J., Pitkänen, T., Cessateur, G., Gunell, H., & Maes, L. (2017). The delayed time response of geomagnetic activity to the solar wind. *Journal of Geophysical Research: Space Physics*, *122*, 11,109–11,127. https://doi.org/10.1002/2016JA023793

Received 9 DEC 2016
Accepted 1 SEP 2017
Accepted article online 5 SEP 2017
Published online 10 NOV 2017

The Delayed Time Response of Geomagnetic Activity to the Solar Wind

R. Maggiolo[1], M. Hamrin[2], J. De Keyser[1], T. Pitkänen[2], G. Cessateur[1], H. Gunell[1], and L. Maes[1]

[1]Belgian Royal Institute for Space Aeronomy, Brussels, Belgium, [2]Department of Physics, Umeå University, Umeå, Sweden

Abstract We investigate the lagged correlation between a selection of geomagnetic indices and solar wind parameters for a complete solar cycle, from 2000 to 2011. We first discuss the mathematical assumptions required for such a correlation analysis. The solar wind parameters and geomagnetic indices have inherent timescales that smooth the variations of the correlation coefficients with time lag. Furthermore, the solar wind structure associated with corotating interaction regions and coronal mass ejections, and the compression regions ahead of them, strongly impacts the lagged correlation analysis results. This work shows that such bias must be taken into account in a correct interpretation of correlations. We then evidence that the magnetospheric response time to solar wind parameters involves multiple timescales. The simultaneous and quick response of the *PC* and *AE* indices to solar wind dynamic pressure with a delay of ~5 min suggests that magnetospheric compression by solar wind can trigger substorm activity. We find that the *PC* and *AE* indices respond to interplanetary magnetic field (IMF) B_Z with a response time of respectively ~20 and ~35 min. The response of the *SYM-H* index takes longer (~80 min) and is less sharp, *SYM-H* being statistically significantly correlated to the IMF B_Z observed up to more than ~10 h before. Our results suggest that the solar wind velocity's dominant impact on geomagnetic activity is caused by the compression regions at the interface of fast/slow solar wind regimes, which are very geo-effective as they are associated with high solar wind pressure and strong interplanetary magnetic field.

1. Introduction

The magnetosphere's interaction with the solar wind is important for many magnetospheric processes, as the solar wind is the primary source for the magnetospheric energy budget. The ratio between the kinetic energy flux and the Poynting flux of the solar wind is approximately 20 at the orbit of Earth (e.g., Koskinen & Tanskanen, 2002). However, only a fraction of the available solar wind kinetic energy is needed to power the magnetospheric dynamics (Koskinen & Tanskanen, 2002). The energy input into the magnetosphere depends on several factors, for example, the solar wind kinetic energy and the configuration of the interplanetary magnetic field (IMF). The magnetosphere responds to solar wind energy input in many ways, e.g., by releasing magnetic substorms and storms, but the responses are generally not instantaneous (Nakamura, 2006). Geomagnetic storms refer to large-scale and intense magnetospheric disturbances leading to injection of an appreciable number of ions and electrons from the tail to the inner magnetosphere leading to a rapid growth of the ring current causing worldwide magnetic perturbations (e.g., Gonzalez et al., 1994). Geomagnetic substorms correspond to transient processes of shorter duration associated with enhanced field-aligned currents and particle precipitation in the nightside auroral region (e.g., Rostoker et al., 1980). To understand how the magnetosphere responds to the solar wind and to the IMF, it is important to identify how energy, momentum, and mass can enter into the magnetosphere and what timescales are involved. These include the inherent timescales of the solar wind and the IMF, the transit timescales for waves and plasma flows, and the timescales of the triggered magnetospheric processes. The magnetospheric response to the solar wind and the IMF is important for our modern society that is increasingly dependent on the space environment. Understanding the timescales at which the magnetosphere responds to the solar wind is important for space weather predictions, and the knowledge can be exploited by space situational awareness programs.

The magnetospheric response to solar wind variations can be probed with geomagnetic activity indices such as the polar cap index (*PC*), the auroral electrojet index (*AE*), and the disturbed storm time index (*Dst*). The *PC* index measures geomagnetic disturbances in the polar cap regions by using magnetometer readings from two stations (Thule in the north and Vostok in the south) (Troshichev & Andrezen, 1985;

Troshichev et al., 1988). This index is a proxy for the energy that enters into the magnetosphere due to solar wind-magnetosphere coupling (International Association of Geomagnetism and Aeronomy recommendation 2013). The auroral electrojet index (*AE*) is obtained from a network of stations in the latitude region that is typical of the northern hemisphere auroral zone (Davis & Sugiura, 1966). It is designed to provide a global, quantitative measure of auroral zone magnetic activity produced by enhanced ionospheric currents flowing below and within the auroral oval. Excursions in the *AE* index from a nominal daily baseline are indicative of substorm activity. The time resolution of both *PC* and *AE* is 1 min. Note that the *PC* and *AE* indices are well correlated (e.g., Takalo & Timonen, 1998). The best correlation between these two indices is found when the *PC* index precedes the *AE* index by 5–15 min (Vassiliadis et al., 1996). The *Dst* index measures the changes in the ring current by using several ground-based magnetometers at equatorial latitudes (Sugiura, 1964). Since the time resolution of *Dst* is low (1 h), the 1 min resolution *SYM-H* index is sometimes used instead of *Dst* (Li et al., 2011; Wanliss & Showalter, 2006). Large negative variations of the *Dst* or *SYM-H* indices are indicative of geomagnetic storm occurrence.

Solar wind energy, momentum, and mass are transferred to the magnetosphere mainly via magnetic reconnection processes at the dayside magnetopause (Paschmann et al., 1979). However, there are also other ways in which solar wind energy, momentum, and mass can enter the magnetosphere, e.g., directly through the cusps (e.g., Kremser & Lundin, 1990), via impulsive penetration of a plasma across the magnetopause (e.g., Gunell et al., 2012), via diffusion at the magnetopause (e.g., Tsurutani & Thorne, 1982), and during periods of northward IMF via the Kelvin-Helmoltz instability (e.g., Hasegawa et al., 2004) and high-latitude reconnection (e.g., Fuselier et al., 2000). Magnetic reconnection is especially favorable for southward IMF conditions (see, e.g., Yamada et al., 2010). The primary magnetospheric convection is expected to be controlled by dayside magnetopause reconnection combined with reconnection at a distant neutral line in the magnetotail, the so-called Dungey cycle (Dungey, 1961). Field lines opened by dayside reconnection convect tailward, and magnetic energy is subsequently stored in the tail magnetic field, in particular, in the lobes. Stored energy can be explosively released during substorms when plasma and magnetic flux are ejected from a near-Earth neutral line toward Earth or into interplanetary space. As a consequence, auroral displays can be observed from the ground as the ionosphere is connected to auroral generators in the magnetotail via magnetic field-aligned currents (Haerendel, 2011). Substorms are also associated with an enhancement of horizontal currents in the auroral ionosphere (the auroral electrojets) which results in an increase of the *AE* index value. Excursions in the *AE* index from a nominal daily baseline are called "magnetospheric substorms" and may have durations from tens of minutes to several hours. The typical *AE* index variation during a substorm consists of an increase of the index during a period of roughly 2 h (which includes the substorm growth phase and the expansion phase) followed by a decrease of the *AE* index typically during 2 h (which corresponds to the recovery phase of the substorm). A detailed discussion of the variations of the auroral indices during substorm phases can be found in Gjerloev et al. (2004).

During geomagnetically active times when energy transfer from the solar wind/IMF into the magnetosphere is sufficiently intense and long lasting, the ring current is enhanced via energization and injections of plasma sheet particles from the tail toward the inner magnetosphere. Such perturbations leading to a significant intensification of the ring current are referred to as geomagnetic storm (e.g., Daglis et al., 1999). Geomagnetic storms are associated with large negative excursions in the *Dst* and the *SYM-H* indices, a consequence of the magnetic field produced by the enhanced ring current. The main phase of a geomagnetic storm corresponds to a decrease of *SYM-H* indicative of an increase in the intensity of the ring current. The decrease of the ring current intensity is associated with an increase of *SYM-H* and is termed as the recovery phase. The main phase typically lasts 6–13 h, while the recovery phase may take much longer, typically tens of hours (see, e.g., Hutchinson et al., 2011; Yokoyama & Kamide (1997)). Yokoyama and Kamide (1997) analyzed more than 300 geomagnetic storms and reported main phase durations ranging from ~5 h to 14 h and recovery phase durations ranging from ~16 to 56 h, respectively for weak storms and intense storms. Some magnetic storms are associated with a short interval of increased *SYM-H* before the storm main phase. This is called the initial phase and the increase of *SYM-H* the storm sudden commencement. It results from an intensification of the magnetopause current caused by a sudden compression of the dayside magnetosphere by increased solar wind dynamic pressure. The duration of an initial phase may vary from a couple of hours to 1 day (e.g., Hutchinson et al., 2011), and its absolute magnitude is low compared to the magnitude of the storm main phase.

The magnetospheric response times to variations in the solar wind and IMF can vary from minutes to days, depending on what physical processes are involved in the Earth's magnetosphere. Some processes in the magnetosphere respond faster to solar wind energy input than others. For example, ultralow frequency (ULF) waves can be observed by ground-based magnetometers rather quickly after the magnetosphere has experienced a rapid compression due to a sudden increase in the solar wind pressure (e.g., Keiling & Takahashi, 2011), reflecting the travel time of the compressional perturbation into the magnetosphere and the time to excite ULF resonances. The time delay between solar wind energy input (e.g., a southward turning of the IMF) and the release of energy in the magnetotail during a substorm is considerably longer, of the order of 30–60 min (e.g., Bargatze et al., 1999; Rostoker et al., 1972). The time delay of effects caused by the dawn-dusk IMF component is under debate (e.g., Browett et al., 2016; Pitkänen et al., 2016; Tenfjord et al., 2015, and references therein). The response time for geomagnetic storms is even longer since it takes a considerably long time to inject particles into the ring current region (e.g., Daglis et al., 1999).

Geomagnetic activity indices have been used for a long time to study the delayed magnetospheric response times to solar wind and IMF variations. However, the response can also be seen in other magnetospheric signatures such as magnetospheric and ionospheric convection flows, plasma densities, and magnetospheric potential drops or electric fields. One of the earlier investigations of the time delay between solar wind variations and geomagnetic activity as measured by a geomagnetic index was conducted by Wilcox et al. (1967). They studied the magnetospheric response as observed by the 3 h resolution planetary *Kp* index, and they concluded that the response occurs within the first 3 h. Meng et al. (1973) used data from the IMP-3 satellite to investigate the cross correlation between the southward IMF component and the *AE* index. They observed a peak correlation for a delayed response time of about 40 min. Bargatze et al. (1985) used solar wind velocity and magnetic field data from the IMP-8 satellite to study the time lag of the magnetospheric response as observed by the *AL* index. Based on a linear prediction filter technique, they argued that the magnetosphere experiences a loading-unloading cycle in response to solar wind variations, and they observed two different response times: a ~ 20 min response time corresponding to magnetospheric processes directly driven by the solar wind activity, and a ~ 60 min response time related to the unloading or release of stored energy in the magnetotail. Baker et al. (1981) also exploited data from the IMP-8 spacecraft to investigate the correlation between the *AE* index and several solar wind parameters and combinations of parameters. They argued that a combination of the solar wind velocity and the IMF correlates best with *AE* and that the time lag is ~40 min. Gonzalez and Tsurutani (1987) studied the response of *Dst* to solar wind variations observed by the ISEE-3 satellite. Intense magnetic storms ($Dst < -100$ nT) were found to occur after large and negative southward IMF and lasting >5 h.

More recently, Newell and Liou (2011) used data from the OMNIWeb and magnetospheric data from Polar Ultra Violet Imager (UVI) and Imager for Magnetopause-to-Aurora Global Exploration (IMAGE) Far Ultraviolet Imager (FUV) and argued that magnetotail effects can be observed in the ionosphere approximately 20 min after the IMF B_Z has had a northward turning. Hairston and Heelis (1995) studied the time-lagged response of polar ionospheric convection patterns with respect to north-south changes in the IMF as observed by the IMP-8 satellite. After removing the transit time from the spacecraft to the magnetopause, they observed a time lag of 17–25 min in the ionospheric flows responding to the IMF changing from northward to southward. Khan and Cowley (1999) also investigated the response time of ionospheric convection to variations in the IMF with data from the European Incoherent Scatter (EISCAT) radars and the IMP-8 satellite. They observed small time delays (only a few minutes); the delay was shortest in the ~1400 magnetic local time (MLT) sector. Aikio et al. (2013) used ACE solar wind data, Geotail data in the magnetosphere, and ground-based data from the EISCAT radars and the Magnetometers - Ionospheric Radars- Allsky Cameras Large Experiment (MIRACLE) magnetometers to study the variations of the magnetotail inclination angle, the location of the polar cap boundary, and the magnetic signature of the convection reversal boundary, with respect to variations in the IMF B_Z component. They estimated a time lag of the response of about 17 min. Boudouridis et al. (2011) also studied effects on the ionospheric convection. They used Geotail and Super Dual Auroral Radar Network data to show that there is an almost immediate response (within a few minutes) to a dynamic pressure pulse hitting the dayside magnetopause during southward IMF. For northward IMF the delay was longer. Enhanced convection flows were observed during 20–30 min (40–50 min) during southward (northward) IMF. Fear and Milan (2012) used solar wind data from the OMNIWeb and FUV camera data from the IMAGE spacecraft to study the IMF dependence of the orientation of transpolar arcs. They observed

correlations between IMF B_Y with time lags of 3–4 h. Borovsky et al. (1998) used ISEE-2 data in a statistical investigation too, and they concluded that the time for the solar wind plasma to reach the midtail plasma sheet, the near-Earth nightside plasma sheet, and the dayside plasma sheet are about 2 h, 4 h, and 15 h. Nagata et al. (2008) also investigated the influence of the solar wind on the plasma sheet density. Using Geotail data, they found that the plasma sheet density depends on the solar wind density and IMF B_Z with a time lag and duration of several hours. Numerical simulations were used by Ebihara and Ejiri (2000) to investigate the response of the ring current density with respect to the solar wind density, and they observed a time delay of ~7 h. The solar wind response of the midtail electric field was investigated by Nakamura et al. (1999) by using data from the Wind and Geotail spacecraft and from ground-based magnetometers. They found that the electric field responded well to the enhanced solar wind energy input with a time delay of 45–80 min. The correlation between the solar wind and cross-polar cap potential drop was studied by Eriksson et al. (2000). Using data from the Wind and FAST spacecraft, a major response was observed with a 15 min time lag, but also later responses with lags of 55–105 min were observed.

As evident from this brief literature review, issues concerning the magnetosphere's response to variations in the solar wind and in the IMF, and issues concerning the delayed response times, have been investigated since the beginning of the space age (see, for example, Arnoldy, 1971; Clauer et al., 1981; Kane, 1972, 1974; Russell & McPherron, 1973). However, still there is no general consensus on the dominant timescales involved and on how inherent scales in the solar wind can influence the experimental determination of magnetospheric response times.

Correlation analysis is a widely used tool to study the coupling between the solar wind and the magnetosphere. A large number of studies already investigated the correlation between solar wind parameters or coupling functions (e.g., Newell et al., 2007, and references therein) obtained from a combination of solar wind parameters and geomagnetic indices. Usually, the physical interpretation of the result is based on the analysis of the magnitude of the correlation coefficient but the magnetospheric response time is not explicitly considered. However, it is indirectly accounted for when low time resolution indices (like the 3 h *Kp* index or the 1 h *Dst* index) or averaged solar wind parameters are used. Furthermore, little attention is paid to the validity of the mathematical assumptions required for a correct correlation analysis and on their impact on the results. The magnitude of the correlation coefficients is thus usually considered as a reliable indicator of the significance of the relation between the solar wind parameters and the geomagnetic indices.

In this paper, we analyze the response times of geomagnetic indices to solar wind conditions by investigating their lagged correlation with the solar wind parameters. To do so, we use high time resolution indices and solar wind parameters over a solar cycle period of 11 years (see section 2). We first check the impact of the nonvalidity of the basic assumptions of the correlation analysis, in particular, the effects of the parameters' autocorrelation and of the solar wind structuring (sections 3.1 and 3.2). We then discuss the lagged correlations between solar wind parameters and indices and their implications for the magnetospheric response times (section 3.3).

2. Data and Method

We make a detailed analysis of the correlation between solar wind parameters and geomagnetic indices over a period of 11 years from 2000 to 2010, starting at the maximum of solar cycle 23 and ending at 2 years after the beginning of solar cycle 24. We make the correlation analysis on this whole time period and do not focus on specific solar wind or geomagnetic conditions.

We consider the *PC* index, the *AE* index, and the *SYM-H* index. We analyze the variations of the linear correlation coefficient between these geomagnetic indices and a set of solar wind parameters during the time periods when all data are available. We consider the IMF magnetic field magnitude (B_{SW}), the B_X, B_Y, and B_Z GSM (geocentric solar magnetospheric) components of the IMF, and the solar wind density (N_{SW}), velocity (V_{SW}), and dynamic pressure (P_{SW}). Both the solar wind data and the geomagnetic indices are extracted from the OMNI data set through the OMNIWeb. We use 5 min resolution solar wind parameters propagated to the nominal magnetospheric bow shock. The details of the method used to compute 5 min averaged data and to propagate solar wind data to the nose of the bow shock can be found on the OMNIWeb website (http://omniweb.gsfc.nasa.gov/). For the 11 year period analyzed in this study, we obtain 1,106,738 five minute samples when both indices and solar wind parameters are available, which

corresponds to 95.6% of the total number of 5 min time intervals. For the correlation analysis, we only consider time periods when all data are available.

We compute the linear correlation coefficient between the solar wind parameters and the indices as a function of the time lag Δt applied between the time when the observed solar wind parameters reach the bow shock and the time when the indices are measured. We investigate the variation of the cross-correlation coefficients between the solar wind parameters and the geomagnetic indices as a function of Δt on a time span of ± 4 days around the time when the indices are measured. The resolution of Δt is limited to 5 min by the use of 5 min averaged data. This choice of a 5 min resolution has been made considering that the typical uncertainty due to solar wind propagation is of a few minutes (e.g., Mailyan et al., 2008) which makes the use of a higher time resolution pointless.

There are several ways of measuring the correlation between variables. In the following we will only use the Pearson correlation coefficient (PCC) (see Pearson, 1920, 1931, 1932) as it is by far the most widely used in space physics. We use the following notation for the delayed correlation between two variables: $C_{X/Y}(\Delta t)$ corresponds to the PCC between the variable $Y(t + \Delta t)$ and the variable $X(t)$. The PCC is a statistical estimator r of ρ, the strength of the linear correlation between X and Y.

The definition of the PCC relies on several mathematical assumptions (e.g., Peat & Barton, 2005), in particular, that the variables have been randomly selected from a general population; that the observations are independent of each other (i.e., the variables are not autocorrelated); and that the relation between the two variables is linear. The PCC can be used with any type of distribution of the variables (as long as the distribution's variance is defined). However, Pearson's correlation coefficient is known not to be a robust estimator, its quality being strongly affected by the underlying distributions, implying also that it is not outlier resistant. For large sample sizes, the PCC is an unbiased estimator for the true correlation ρ. For small sample sizes one should be careful, since the PCC then is biased. When considering a dependence of a variable (the "output" variable) on multiple other variables (the "input" variables), Pearson's analysis applied for each input variable separately represents a reliable measure of the strength of the linear correlation between the output and each input variable separately, only if the input variables are statistically independent.

After determining the PCC, it is necessary to check its significance. Two situations are typically considered: (a) testing the probability of obtaining a nonzero correlation coefficient by chance while the two variables are not correlated; and (b) establishing a confidence interval for the estimator r that contains the true correlation coefficient ρ. Significance checks have been developed for both situations for normally distributed data. As already mentioned, the PCC is not a robust estimator and thus one should be very careful while interpreting the PCC for nonnormally distributed data.

The significance of the PCC for the first type of significance check depends on the number of degrees of freedom of the system ($N - 2$, where N is the number of data points used to compute the Pearson correlation coefficient) and on the value of the cross-correlation coefficient. It turns out that the value $t = r((N - 2)/(1 - r^2))^{1/2}$ follows Student's t distribution for the case of zero correlation. The significance level for a given cross-correlation coefficient and a given number of data points can thus be obtained from tables providing the critical values of the PCC derived from the statistical t test. For a large data set ($\sim > 1000$ independent points) as in our case, the 99% confidence level for the PCC (for a two-tailed test, i.e., with no a priori knowledge of the sign of the correlation coefficient) is reached when the absolute value of the cross-correlation coefficient r is higher than 0.114. This study does not aim at making predictions but rather at identifying solar wind parameters that impact geomagnetic activity. In consequence, we discuss correlation coefficients that are statistically significant (i.e., higher than 0.114) even if they only account for a relatively small part of the variability of geomagnetic indices as estimated from the Pearson analysis (the same argument applies to the solar wind parameters intercorrelation).

The determination of the significance is affected by the violation of the mathematical assumptions associated with the Pearson analysis (e.g., see Edgell & Noon, 1984, and references therein). The following mathematical assumptions are usually not satisfied in space physics:

1. The solar wind and geomagnetic indices are far from being normally distributed. For example, the solar wind speed has a typical binary distribution (slow and fast wind). The same is true for B_X and B_Y that

follow an inward or outward Parker spiral orientation. Other variables like P_{SW}, N_{SW}, and B_{SW} cannot be normally distributed since they have to be >0.

2. The PCC estimates a possible linear correlation, which is then believed to reflect solar wind-magnetosphere coupling. It is not a priori known whether such a linear correlation exists; in fact, it is known that different regimes exist. Indeed, the most important variations of the *PC*, *AE*, and *SYM-H* indices, developed to monitor geomagnetic activity, occur during active periods. During nonactive periods, these indices display very weak variations and have a low absolute value. As already mentioned, the determination of the PCC is strongly affected by outliers (e.g., Anscombe, 1971), i.e., by data points whose values strongly differ from the nominal parameter values. Consequently, quiet periods have a weak impact on the correlation results, as the overall correlation is mostly dominated by the correlation between solar wind parameters and indices during active periods. From a simple conditional search on the *AE* and *SYM-H* indices in our data set, we estimated the total number of 5 min data points taken during substorms (defined as periods when *AE* is higher than 400 nT) and during magnetic storms (defined as periods when *SYM-H* is lower than -50 nT) to be respectively 153,816 and 45,307. The value of the PCC will mostly depend on data taken during these time periods, even if they represent a small fraction of the 11 years of data analyzed in this study (respectively 13.3% and ~4%) This illustrates that the mixture of different regimes in the input data might lead to a result that actually reflects the behavior of only a subset of the data. Note that the subset of data corresponding to active periods is still large from a statistical point of view. If only these periods were considered, the 99% confidence level for the correlation coefficient would not differ from the one for the whole time period.
3. Successive data points for a given parameter are not statistically independent from one another as evident from the parameter's autocorrelation time. This autocorrelation reflects the structure of the solar wind parameter or of the geomagnetic index: both kinds of parameters follow specific underlying physical structures. A consequence is that the effective number of degrees of freedom is much less than *N*.
4. The PCC correlates exact data from two different distributions. In reality, we deal with measured data. There are clearly error margins on the solar wind measurements in the OMNI database. Similarly, there are errors associated with the geomagnetic indices. These include, for example, measurement errors (e.g., on the magnetometer readings going into the determination of *AE*) but also sampling errors (e.g., since the *AE* is based on measurements at only a handful of stations, it represents a geometrical sampling of auroral electrojet perturbations). Such errors are difficult to quantify and are often not available for space physics data. They have a detrimental effect on the capacity to establish correlations, even for large data sets. While constant errors on the data do not affect the determination of the correlation coefficient, random errors will always lead to an underestimation of the significance of a correlation as they increase the standard deviation of the data.

It is possible to remedy, at least partially, the above limitations. This can be done, for instance, by introducing nonlinear transformations of the parameters in order to obtain normally distributed input and output variables or by breaking up the data set in "quiet" and "active" times to establish separate correlations for the different regimes and limit the impact of outliers on the results. Furthermore, special methods have been developed for nonlinear systems. For instance, the NARMAX (Nonlinear AutoRegressive Moving Average with eXogenous input) model has been successfully applied to model the evolution of energetic electron fluxes in geostationary orbit (Balikhin et al., 2011) or to identify the most influential functions for the solar wind-magnetosphere coupling (Boynton et al., 2011). However, such methods are more complex to implement and are rarely used in space physics.

In this study, we have chosen to use the more simple Pearson correlation analysis. Our aim is to show that by carefully taking into account the effect of the nonfulfillment of the required mathematical assumptions, it is possible to extract pertinent physical information. At the same time we identify the possible impact of the limitations of the Pearson analysis on previously published results. We show that the autocorrelation of solar wind parameters, the autocorrelation of geomagnetic indices (see section 3.1), and the cross correlation between solar wind parameters (see section 3.2) strongly influence the variation of the cross-correlation coefficient between solar wind parameters and indices as a function of the time lag Δt, and this can affect our understanding of the lagged correlation between solar wind parameters and geomagnetic indices.

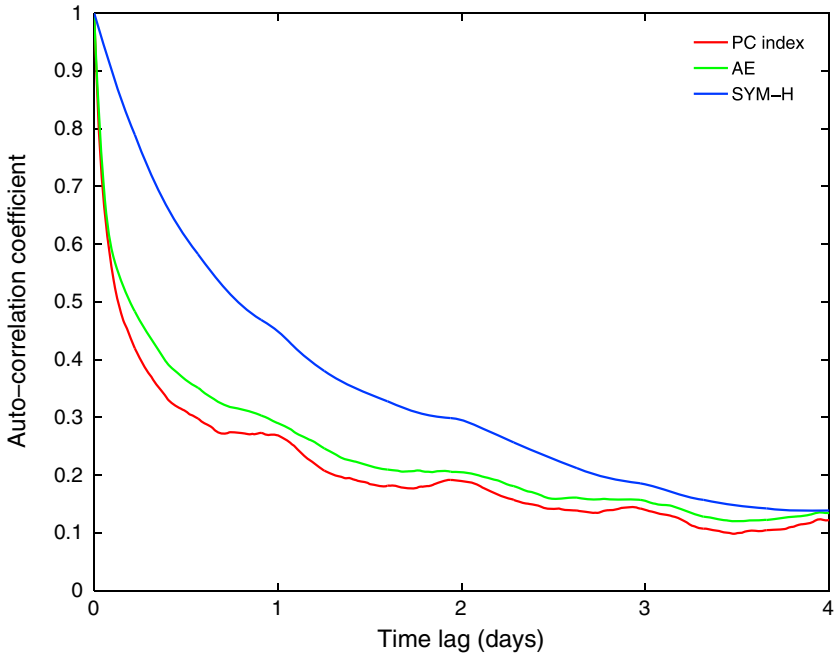

Figure 1. Autocorrelation coefficient for the *PC*, *AE*, and *SYM-H* indices.

3. Observations

3.1. Inherent Timescales (Autocorrelation)

Each solar wind parameter and index has its own autocorrelation time. These times are important as they lead to a smoothing of the variation of the cross-correlation coefficient with the time lag Δt; correlation peaks cannot be narrower than the largest of the autocorrelation timescales of both variables under consideration.

Figure 1 displays the autocorrelation coefficient for each index, i.e., the correlation between the index $I(t)$ and $I(t + \Delta t)$. We define the autocorrelation time τ as the value of the time lag Δt for which the autocorrelation coefficient is equal to 0.5, half its maximal value of 1 at $\Delta t = 0$. The autocorrelation time for each of the solar wind parameters and indices used in this study are summarized in Table 1.

3.1.1. *PC* and *AE* Indices

As expected from their high correlation (e.g., Takalo & Timonen, 1998), the *PC* and *AE* indices have relatively similar autocorrelation times (τ_{PC} = 185 min or ~3 h and τ_{AE} = 280 min or ~4.5 h). The τ_{AE} is in good agreement with the typical duration of of periods when the *AE* index significantly differs from its nominal quiet time value during substorms (e.g., Russell & McPherron, 1973). However, *AE* index variations due to substorm activity may be slightly higher than the actual duration of substorms. Chu et al. (2015) estimated that the most probable duration of subtorm is of the order of ~40 min and suggested that the longer duration of the variation of the *AL* index (from which is derived *AE*) is because it not only measures the westward electrojet of the substorm current wedge but also variations of the high-latitude convection.

3.1.2. *SYM-H* Index

The autocorrelation time of *SYM-H* is much longer ($\tau_{SYM\text{-}H}$ = 1130 min or ~19 h) and is consistent with the typical duration of the significant negative excursion of *SYM-H* during magnetic storms (e.g., Yokoyama & Kamide, 1997), and it corresponds to the lifetime of storm time ring current enhancements. In consequence, the correlation between solar wind parameters and *SYM-H* will display smoother variations with Δt compared to the *PC* and *AE* indices. Note that the three indices in Figure 1 show a weak 1 day modulation of the autocorrelation coefficient related to ground magnetic field periodic variations due to the Earth's rotation and the uneven sampling of the magnetic field by only a handful of ground-based observatories.

Table 1
Autocorrelation Times (in Minutes) for the Geomagnetic Indices and the Solar Wind Parameters

	Autocorrelation Time (min)
PC	185
AE	285
SYM-H	1125
B	825
B_X	610
B_Y	305
B_Z	80
V	2690
N	540
P	385

Note. The autocorrelation time corresponds to the time lag Δt for which the autocorrelation coefficient is equal to half its maximum value (i.e., 0.5).

3.1.3. IMF GSM Components

The autocorrelation coefficients of the solar wind parameters are shown in Figure 2. The IMF GSM components have a relatively short autocorrelation time. The shortest is for B_Z (τ_{Bz} = 80 min), while it is longer for B_X and B_Y (τ_{Bx} = 610 and τ_{By} = 305 min). These different autocorrelation times can be understood by considering the average configuration of the heliospheric magnetic field. For the unperturbed solar wind at Earth's orbit, near the solar equatorial plane, there is no privileged orientation for B_Z while the average B_X and B_Y orientation is given by the Parker spiral. The B_Z component varies due to the sector structure of the heliospheric field, and it is affected by waves or other disturbances, while B_X and B_Y are distributed around two modal values, one positive and one negative, depending on which side of the heliospheric current sheet Earth is located (see Russell, 2001). Consequently, B_Z variations, and in particular, changes of its sign, occur on shorter timescales compared to B_X and B_Y sign changes which require a crossing of the heliospheric neutral sheet.

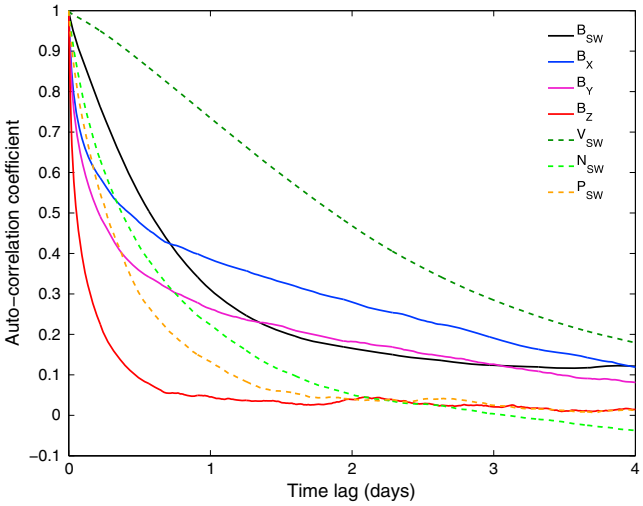

Figure 2. Autocorrelation coefficients for the solar wind parameters.

3.1.4. Solar Wind Velocity, Density, and Dynamic Pressure

The solar wind velocity has the longest autocorrelation time ($\tau_V \sim 44$ h). The typical solar wind velocity at Earth (~450 km/s) corresponds to the equatorial slow solar wind regime associated with the equatorial coronal streamer belt (e.g., Tokumaru et al., 2010). The most dramatic changes of the solar wind velocity at Earth almost exclusively correspond to increases in the solar wind speed. There are two principal sources of high-speed solar wind, coronal holes, and coronal mass ejections (CMEs). High-speed solar wind streams of typically 500–800 km/s emanate from coronal holes and thus often corotate with the Sun over several solar rotations as coronal holes evolve slowly. CMEs are huge bubbles of coronal plasma ejected from the Sun over the course of several hours (Brueckner, 1974; Gosling et al., 1974; MacQueen et al., 1974; Tousey, 1973). While many CMEs travel at a velocity close to the nominal solar wind velocity, some of them propagate at very high velocities, up to more than 2000 km/s (e.g., Cane & Richardson, 2003; Jian et al., 2006; Lindsay et al., 1999; Liou et al., 2014). Both high-speed streams and CMEs are large-scale structures and result in long-lasting periods (several hours to some days) of high solar wind velocity, and they are responsible for the long autocorrelation time of the solar wind velocity.

High-speed solar wind flows are associated with a decrease in the solar wind density for long time periods (e.g., McComas et al., 2000). However, the solar wind density also varies at smaller timescales, for instance, at stream interfaces where it increases in a few hours as it passes over a probing spacecraft (e.g., Forsyth & Marsch, 1999). Consequently, the autocorrelation time for the density ($\tau_N \sim 9$ h) is lower than for the velocity. The solar wind dynamic pressure, whose fluctuations can be due to both solar wind velocity and density variations, necessarily has an even shorter autocorrelation time ($\tau_P \sim 6.5$ h).

3.2. Solar Wind Structure (Cross Correlation of Solar Wind Parameters)

In addition to the parameters' autocorrelation, a second limitation to the cross-correlation analysis between the solar wind parameters and the indices stems from the fact that the solar wind parameters are not statistically independent among themselves. Consequently, a proper understanding of their cross correlation is required before interpreting their relation with the geomagnetic indices.

3.2.1. Correlations With Solar Wind Speed

The cross correlation between the solar wind parameters and the magnitude of the solar wind velocity, V_{SW}, as a function of time lag is presented in Figure 3. The time lag Δt corresponds to the time lag applied between the solar wind parameters and the solar wind speed. For each time lag, Δt, the cross-correlation coefficient represents the PCC between a given solar wind parameter as measured at a time t and the solar wind speed measured at a time $t + \Delta t$. It can be written as $C_{X/V}$, where the subscript X represents a solar wind parameter. In other words, positive (negative) Δt for $C_{X/V}$ corresponds to a correlation between the solar wind speed V_{SW} and another solar wind parameter measured earlier (later). Figure 3 shows that these cross correlations are significant so that these solar wind parameters cannot be considered as independent, except for the IMF B_X, B_Y, and B_Z components, which show no correlations with solar wind speed. The solar wind density, kinetic pressure, and the IMF magnitude are, on the contrary, well correlated with the solar wind speed. Their cross-correlation coefficient with solar wind speed displays a bipolar variation as a function of Δt with a maximum for positive Δt and a minimum for negative Δt. Such a variation of the correlation coefficient is the signature of the structuring of the solar wind.

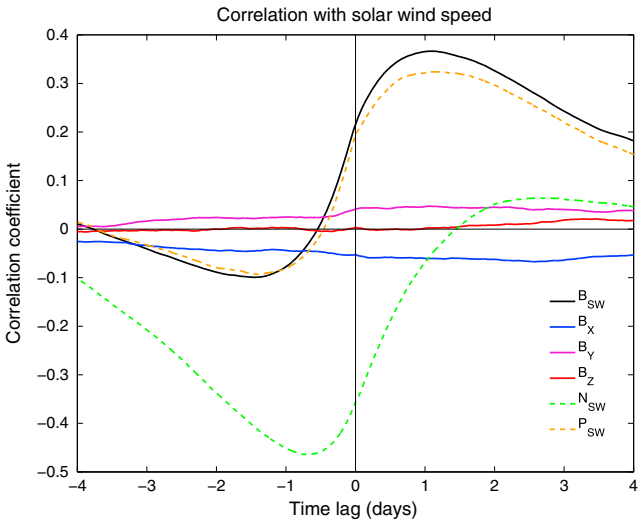

Figure 3. Variation of the correlation coefficients between solar wind parameters and the solar wind speed as a function of the time lag Δt.

As the Pearson correlation coefficient is strongly impacted by outliers, the correlation between solar wind parameters and the solar wind speed mostly represents the effect of structures associated with solar wind speed significantly diverging from the standard one, i.e., the effect of fast CMEs

and high-speed solar wind streams. The impact of other large-scale solar wind disturbances not associated with significant solar wind speed changes may not be visible in Figure 3.

When fast CMEs and high-speed solar wind streams propagate in the heliosphere, they interact with the surrounding slower solar wind. Corotating interaction regions (CIR) refer to regions where high-speed solar wind streams interact with a slower solar wind region. The ensuing structuring is discussed by Borovsky and Denton (2010). The fast flow interacts with the slower solar wind in front of it and compresses it. The compression region is characterized by a high magnetic field, density, and pressure. Typically, the density increase is observed when the solar wind velocity starts to increase. A few hours after the density peaks (typically 2 h), the magnetic field magnitude and solar wind dynamic pressure peak. Finally, the velocity is maximum approximately 1 day after it started to increase, this high velocity region being associated with a lower solar wind density. Fast CMEs are preceded by a compression region that is associated with a higher plasma density and magnetic field producing a structure that is globally similar to that of CIRs (e.g., Gopalswamy, 2008).

In order to check that the cross correlation of solar wind parameters with solar wind velocity was mostly controlled by CMEs and CIRs events, we repeated this analysis for a subset of events corresponding to CMEs and CIRs. It is the only time in this study that we make a preselection of data prior to performing the correlation analysis. We computed the cross-correlation coefficients of solar wind parameters for subperiods when CIRs (27 events from the list of Borovsky & Denton, 2010) or CMEs (242 events from the list of Richardson and Cane available at http://www.srl.caltech.edu/ACE/ASC/DATA/level3/icmetable2.htm) have been identified. The results for these two subsets of events (see supporting information) are very similar to the result for the whole time period, indicating that the structuring of solar wind parameters evidenced in Figure 3 is actually mostly due to the interaction of fast CMEs and CIRs with the surrounding slower solar wind and that the solar wind structuring caused by fast CMEs and CIRs is indeed globally similar.

3.2.1.1. Correlation of Solar Wind Dynamic Pressure and the IMF Magnitude With Solar Wind Speed

As can be seen from Figure 3, the cross-correlation coefficient of solar wind pressure ($C_{P/V}$) and magnetic field magnitude ($C_{B/V}$) with solar wind speed peaks for positive $\Delta t \sim 1$ day, with correlation coefficients well above the 99% significance level ($C_{P/V} = 0.32$ and $C_{B/V} = 0.37$). This means that periods of high solar wind speeds are statistically preceded by an increase of B_{SW} and P_{SW} occurring approximately 1 day before, in good agreement with the structuring of CIRs and high-speed CMEs, and reflecting how the frozen-in IMF is compressed ahead of a solar wind speed increase. $C_{P/V}$ and $C_{B/V}$ also display a negative peak for $\Delta t \sim -1.5$ day whose maximum magnitude ($C_{P/V} = -0.09$ and $C_{B/V} = -0.10$) is smaller than the positive peak observed at $\Delta t \sim 1$ day and is slightly below the 99% confidence level. It is also interesting to note that $C_{P/V}$ and $C_{B/V}$ follow a very similar variation with Δt. However, one has to keep in mind that the solar wind speed has a long autocorrelation time (44 h) which is smoothing the cross-correlation coefficient variation with Δt and does not allow us to determine small time differences. We will show later that B_{SW} and P_{SW} variations are actually delayed. The long autocorrelation time of V_{SW} may also impact the determination of the location of the peaks of the cross-correlation coefficient. Indeed, the positive and negative peaks of $C_{P/V}$ and of $C_{B/V}$ are separated by ~2.5 days, which is comparable to the solar wind speed autocorrelation time. In Figure 3, we can note that the variation rate of $C_{P/V}$ and of $C_{B/V}$ between their negative and positive peaks (a variation of a factor of 2 in ~1 day or 24 h) is higher than the minimum one expected from the velocity autocorrelation time (a variation of a factor of 2 in ~2 days or 44 h) and higher than the variation rate of $C_{P/V}$ and $C_{B/V}$ before the first peak and after the second peak. Consequently, the magnitude and time lag of those two peaks may be biased; in particular, their magnitude may be artificially decreased and their position shifted to lower (higher) Δt for the left (right) peak.

3.2.1.2. Correlation of Solar Wind Density With Solar Wind Speed

Similarly, the variation with Δt of the cross-correlation coefficient between the solar wind density and solar wind speed ($C_{N/V}$) may also be impacted by the long autocorrelation time of the solar wind speed. Indeed, in Figure 3, $C_{N/V}$ displays a clear peak (-0.46) at $\Delta t \sim -16$ h, indicative of a decrease of the solar wind density on average ~ -16 h after the solar wind speed increases (hence, a negative value of the peak), which is typical of the transition to a high-speed solar wind regime. Wing et al. (2016) obtained a similar result for the delayed correlation between the solar wind speed and density for the period 2000–2014, with a negative peak for a $\Delta t \sim -17$ h but a slightly different one for the period 1989–2009 with a negative peak for a $\Delta t \sim -14$ h. This indicates that the correlation between the solar wind velocity and density, and maybe more generally the cross correlation of solar wind parameters, depends on the time period under consideration. However, we only observe a small positive peak of $C_{N/V}$ for positive Δt, below the 99% significance level (0.06 at

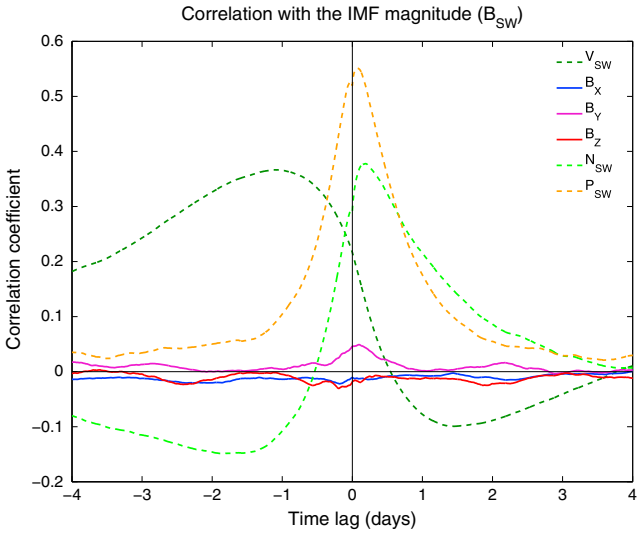

Figure 4. Variation of the correlation coefficients between solar wind parameters and solar wind magnetic field magnitude as a function of the time lag Δt.

Δt ~ 65 h). This peak is weaker and occurs at higher time lags than expected from the typical structure of CIRs and fast CMEs which should be preceded by a density peak about ~1 day before the velocity reaches its maximum (e.g., Borovsky & Denton, 2010). It is likely that the positive peak of $C_{N/V}$ is actually partly hidden because of the strong negative peak of $C_{N/V}$ that may decrease its magnitude and shift it to higher Δt. Finally, we note that none of the IMF components shows a significant correlation with the solar wind velocity, confirming that the orientation of the IMF is not related to the solar wind velocity.

3.2.2. Correlations With IMF Magnitude

Figure 4 shows the cross-correlation coefficient of solar wind parameters with the solar wind magnetic field magnitude B_{SW} as a function of Δt in the same format as Figure 3. This plot highlights the cross-correlation coefficients associated with large deviations of the IMF magnitude from its average value, in particular, the compression regions associated with high-speed solar wind flow and CMEs. We can notice that, except for V_{SW}, the cross-correlation peaks are much sharper than in Figure 2 due to the shorter autocorrelation time of B_{SW} compared to V_{SW} (see Figure 2).

3.2.2.1. Correlation of Solar Wind Pressure With IMF Magnitude

The most prominent peak appears for the cross correlations between the solar wind dynamic pressure and the solar wind magnetic field magnitude ($C_{P/B}$ = 0.55). This is consistent with the strong similarity of the B_{SW} and P_{SW} correlation coefficients with solar wind speed shown in Figure 3. The $C_{P/B}$ peak occurs for Δt ~ 105 min, indicating that a solar wind pressure increase actually precedes a magnetic field increase by about ~105 min, a delay too short to be visible in Figure 3 because of the long autocorrelation time of V_{SW}. This is in agreement with the result of a superposed epoch analysis of interplanetary conditions during geomagnetic storms (including CMEs and CIRs) by Yermolaev et al. (2010), where the solar wind dynamic pressure appears to peak a few hours before the IMF magnitude.

3.2.2.2. Correlation of Solar Wind Density With IMF Magnitude

The second most important peak appears for the cross correlation between the solar wind density and magnetic field magnitude ($C_{N/B}$ = 0.38). It is observed at a Δt ~ 270 min and indicates that density increases precede B_{SW} increases by ~4.5 h, in good agreement with the structuring of CIRs as reported by Borovsky and Denton (2010). At Δt ~ −1.5 days $C_{N/B}$ displays a significant but relatively weak negative peak ($C_{N/B}$ = −0.15) indicative of a decrease of the solar wind density following high IMF magnitude. This is again in agreement with CIR structure where the fast solar wind flow, maximum on average 1 day after the IMF magnitude increase in the compression region, is associated with lower solar wind density. This negative peak is also more extended in time than the positive one, as is the region of low solar wind density in a CIR compared to the region of high solar wind density preceding it. However, this result slightly differs from what was expected from Figure 3. This is a good illustration of the difficulty of correlation analysis. Indeed, the correlation between N_{SW} and V_{SW} clearly evidences the density decrease associated with high-speed solar wind (the strong negative peak of $C_{N/V}$ in Figure 3) while, as discussed above, the location of this peak may be shifted to lower negative Δt. The decrease of N_{SW} with V_{SW} is also evidenced in Figure 4, but in that case it is associated with a relatively weak peak of $C_{N/V}C_{N/V}$. The contrary occurs for the peaks associated with the density increase preceding high-speed stream which is more visible in Figure 4 than in Figure 3. This results from the long autocorrelation time of V_{SW} (see above) and also from the fact that the N_{SW} and B_{SW} increase associated with high-speed solar wind occur on similar timescales (see Figure 4 of Borovsky & Denton, 2010) and are more directly related as they are both associated with the compression front produced by high-speed solar wind.

3.2.3. Conclusions (Solar Wind Structure)

We have shown that the solar wind is structured and that its parameters are significantly correlated. Despite the limitations of such a correlation analysis, we have demonstrated that it is possible to evidence the global structuring of the solar wind by analyzing the correlation coefficient variations with time lag. In particular, it appears that the correlation between the solar wind parameters mostly results from the structuring related to large-scale solar wind disturbances caused by high-speed solar wind streams and CMEs. This is actually not

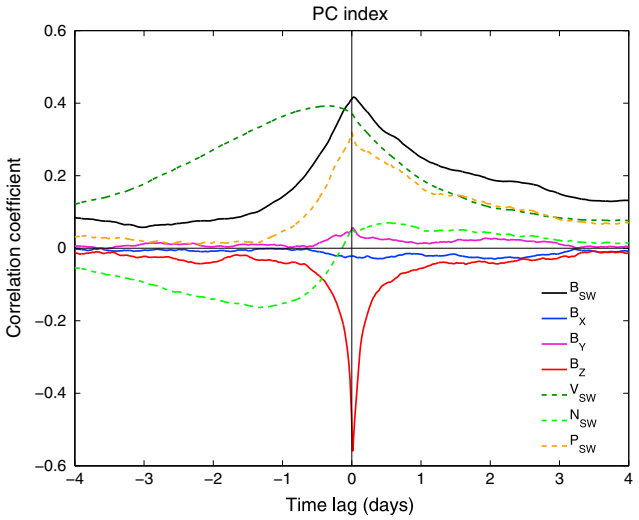

Figure 5. Variation of the correlation coefficients between solar wind parameters and the *PC* index as a function of the time lag Δt.

surprising as both correspond to periods when the solar wind parameters reach their most extreme values, far from the average solar wind conditions. These periods thus have a strong impact on the solar wind parameter cross correlations and autocorrelations, even if they correspond to only a limited fraction of the time period analyzed in this study (during the period considered in this study the average solar wind speed is of 445 km/s and solar wind speed higher than 500 (1000) km/s represent ~27 (~0.001) % of the data set).

3.3. Response Times of Geomagnetic Indices to the Solar Wind Parameters

The following section discusses the cross correlations between solar wind parameters and geomagnetic indices and the impact of solar wind structuring on them. Since CIRs and CMEs are the most common and the most geo-effective large-scale structures in the solar wind (e.g., Borovsky & Denton, 2006; Denton et al., 2006; Gonzalez et al., 1999; Hutchinson et al., 2011; Keesee et al., 2013), it will be necessary to take into account the influence of solar wind parameter cross correlations on the cross correlation between solar wind parameters and geomagnetic indices.

3.3.1. Correlation Between Solar Wind Parameters and the *AE* and *PC* Indices

Figures 5 and 6 display the cross-correlation coefficients between the solar wind parameters and the *PC* and *AE* indices, respectively, as a function of the time lag Δt, in the same format as Figures 3 and 4.

A quick comparison between these two figures reveals that the variation of the *PC* and *AE* cross-correlation coefficients with solar wind parameters is similar, as expected from the high degree of correlation between these two indices (e.g., Vennerstrøm et al., 1991).

3.3.1.1. Correlation With IMF *Bz*

For both indices, the best correlation is found with IMF B_Z ($C_{Bz/AE} = -0.51$ and $C_{Bz/PC} = -0.56$). B_Z displays a negative peak of the correlation coefficient for $\Delta t = 35$ min (*AE* index) and $\Delta t = 20$ min (*PC* index). This 15 min difference for the time of maximum correlation is in good agreement with the fact that these two indices show the best correlation when they are delayed by 5–15 min (Vassiliadis et al., 1996). No significant correlation is found with the IMF B_Y and B_X components.

The $C_{Bz/AE}$ and $C_{Bz/PC}$ peaks are symmetric and sharp, with a half width at half maximum of approximately 3 h, which is comparable to the autocorrelation time of the *AE* and *PC* indices. This is indicative of a quick response of the *AE* and *PC* indices to a southward turning of the IMF.

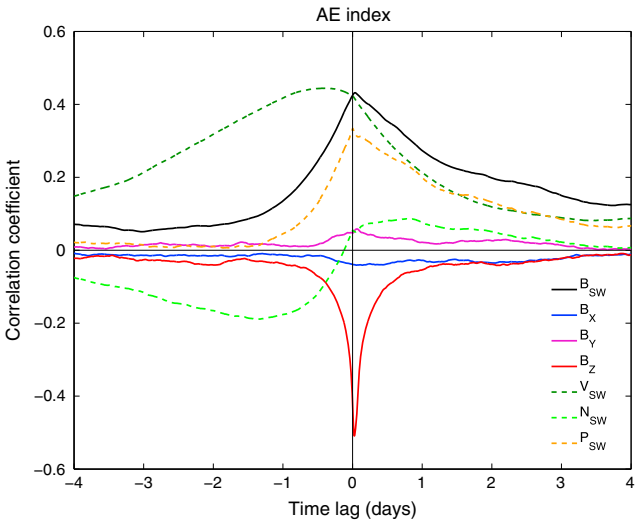

Figure 6. Variation of the correlation coefficients between solar wind parameters and the *AE* index as a function of the time lag Δt.

3.3.1.2. Correlation With IMF Magnitude

The *AE* and *PC* indices are also well correlated with the IMF magnitude. The correlation is maximum for a time lag of 40 min for the *PC* index ($C_{B/PC} = 0.42$) and of 50 min for the *AE* index ($C_{B/AE} = 0.43$), again in agreement with the typical delay between the variations of these two indices. As the *PC* and *AE* indices are correlated to the B_Z component of the IMF and not to the B_Y and B_X components as shown in Figures 5 and 6, we suggest that the high values of $C_{B/PC}$ and $C_{B/AE}$ are mainly due variations in the B_Z component of the IMF. This is consistent with the fact that the delays for the correlation peaks for B_{SW} and B_Z are relatively similar. Such a correlation is expected as a stronger negative IMF B_Z is associated with stronger dayside reconnection, a stronger energy transfer from the solar wind to the magnetosphere, and thus an increased intensity and occurrence probability of substorms, in agreement with the open magnetosphere model of Dungey (1961).

Contrary to $C_{Bz/PC}$, the peaks of $C_{B/AE}$ and $C_{B/PC}$ are not symmetric. The left side of the peak shows a strong decrease rate, consistent with the relatively short autocorrelation timescales of the indices and B_{SW}. On the contrary, their half width at half maximum for high Δt (i.e., on the right side of the

peak) is high, about 1 day and a half, which is much higher than the B_{SW} and the *AE* and *PC* autocorrelation times. For a Δt of 2 days, $C_{B/AE}$ and $C_{B/PC}$ are approximately equal to 0.2, well above the 99% significance level. This signals a correlation between the magnitude of the IMF during the preceding days, independently of its orientation and the *AE* and *PC* indices. One possible reason for this may be that southward IMF turnings often result from a change of the IMF orientation not necessarily associated with a change of its magnitude. Consequently, if an IMF southward turning occurs during a period of high IMF magnitude, it will more likely be associated with a strong negative IMF B_Z, which more readily produces strong variations of the *PC* and *AE* indices. However, from a statistical point of view, we cannot exclude an effect directly related to the IMF magnitude, independently of its orientation.

3.3.1.3. Correlation With Solar Wind Dynamic Pressure

The solar wind dynamic pressure P_{SW} also shows a good correlation with the *AE* and *PC* indices. For both indices, the correlation coefficient sharply peaks for Δt = 5 min, the minimum time lag that can be identified, reaching a value of respectively 0.33 and 0.32. As these values are lower than the maximum correlation between *AE* and *PC* and B_{SW}, one might assume that the correlation with P_{SW} results from the fact that P_{SW} is correlated to B_{SW} and that P_{SW} has actually no direct impact on these indices. However, the timing of the peaks contradicts this hypothesis. First, the maximum correlation for B_{SW} occurs at higher Δt than the maximum correlation for P_{SW}, while from the correlation between solar wind pressure and magnetic field magnitude (Figure 3) we would expect the opposite. Furthermore, contrary to B_Z and B_{SW} for which the maximum correlation occurs at lower Δt for the *PC* index than for the *AE* index (respectively 15 and 10 min), the maximum correlation of P_{SW} occurs at the same Δt = 5 min for both indices. This 5 min delay corresponds to the propagation time of the perturbations produced by interplanetary shocks from the Earth bow shock, where the OMNI solar wind parameters have been propagated, to the ground (e.g., Villante et al., 2004). The simultaneous and quick response of the *AE* and *PC* indices to solar wind pressure shows that magnetospheric compression has a rapid impact on these indices suggesting that solar wind pressure pulse can in some cases trigger substorm activity on short timescales as reported by, e.g., Brittnacher et al. (2000). However, the simultaneous and quick response of indices can also result from other impacts of the solar wind pressure on magnetospheric dynamics not necessarily associated with the full development of substorms. These could correspond to global enhancement of ionospheric currents on short timescales (e.g., Zesta et al., 2000) or flux closure directly driven by the solar wind compression independent of the usual substorm expansion (Hubert et al., 2006). As for B_{SW}, the peak of the correlation between P_{SW} and *AE* and *PC* is asymmetric, displaying a slow decrease for large Δt. For sufficiently large Δt, the correlation coefficients for B_{SW} and P_{SW} display a similar profile with a similar decrease rate, the correlation coefficient for P_{SW} being approximately half of the correlation coefficient for B_{SW}. While it cannot be excluded that this results from a direct effect of P_{SW} on these indices, it seems likely that the slow decrease of $C_{P/AE}$ and $C_{P/PC}$ at large Δt only results from the strong correlation observed between the solar wind magnetic field and pressure ($C_{P/B}$ = 0.55).

3.3.1.4. Correlation With Solar Wind Velocity and Density

Finally, the solar wind velocity and density also display a statistically significant correlation with the *AE* and *PC* indices. The highest correlation between V_{SW} and *AE* and *PC* occurs for negative Δt ($C_{V/AE}$ = 0.44 at $\Delta t = -545$ min and $C_{V/PC}$ = 0.39 at $\Delta t = -535$ min). Similarly, the cross correlation between N_{SW} and the *AE* and *PC* indices is strongest for large negative Δt ($C_{N/AE} = -0.19$ at $\Delta t = -1920$ min and $C_{N/PC} = -0.16$ at $\Delta t = -1935$ min). Note that there is also a positive peak of $C_{N/AE}$ and $C_{N/PC}$ for positive Δt, but it is below the 99% confidence level.

These peaks of the correlation coefficient for large negative Δt (about 9 h for V_{SW} and 32 h for N_{SW}) indicate a correlation between indices and the solar wind velocity and density as measured several hours after the indices. This does not imply a direct effect of *AE* and *PC* on the solar wind velocity and density as that would be in contradiction with the causality principle. It is rather indicative of an indirect link between these indices and solar wind density and velocity, which can easily be understood when considering the structuring of the solar wind and the cross correlation between solar wind parameters as discussed in the previous section. It actually means that *AE* and *PC* variations are correlated with a structure of the solar wind located ahead of fast CMEs and CIRs, i.e., the compression front ahead of fast CMEs and CIRs associated with large B_{SW} and P_{SW}. Indeed, B_{SW} and P_{SW} are actually correlated with *PC* and *AE*, and the solar wind velocity and density are correlated to B_{SW} and P_{SW}. The large negative Δt (about 9 h for the V_{SW} and 32 h for N_{SW}) for which the maximum correlation between V_{SW} and N_{SW} with *AE* and *PC* is observed is globally consistent with the

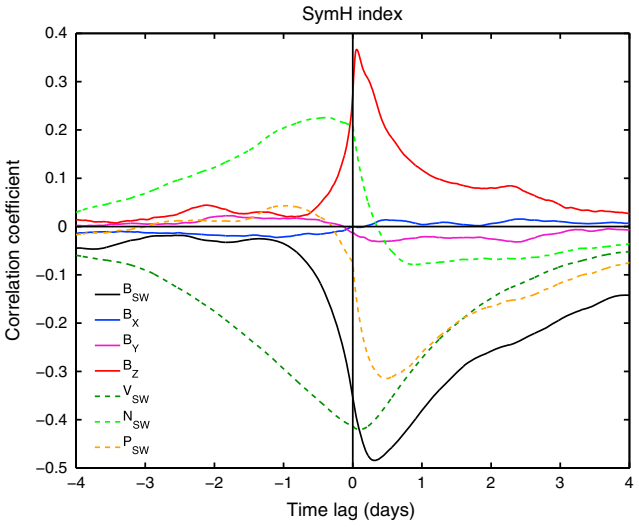

Figure 7. Variation of the correlation coefficients between solar wind parameters and the *SYM-H* index as a function of the time lag Δt.

solar wind structuring evidenced in Figure 4 where a positive peak of $C_{V/B}$ occurs at $\Delta t \sim -1$ day and a negative peak of $C_{N/B}$ occurs at $\Delta t \sim -1.5$ day.

3.3.1.5. Conclusions (Correlation Between Solar Wind Parameters and the *AE* and *PC* Indices)

These results illustrate the impact of the solar wind structuring on the interpretation of the correlation between solar wind parameters and geomagnetic indices such as the *AE* and *PC* indices. If time shifting and solar wind structuring were not considered, the high correlation between V_{SW} and *AE* and *PC* indices for $\Delta t = 0$ ($C_{V/AE} = 0.42$ and $C_{V/PC} = 0.37$) may be interpreted as a direct effect of solar wind velocity on the energy that enters the magnetosphere (*PC* index) and on the intensity and occurrence of substorms (*AE* index), while it rather results from the superposed effect of the cross correlation between V_{SW} and P_{SW} and B_{SW} and from the long autocorrelation time of V_{SW}.

Even for parameters that appear to be directly correlated to the *AE* and *PC* indices, like B_Z, the correlation for $\Delta t = 0$ can be high ($C_{Bz/PC} = -0.42$ and $C_{Bz/PC} = -0.48$) even if the maximum correlation is observed for $\Delta t \neq 0$ because the autocorrelation time of these parameters and of the indices is longer than the time lag corresponding to the maximum correlation.

We found a strong correlation between IMF B_Z and the *AE* index, sharply peaking at $\Delta t = 35$ min. As we find no significant correlation between IMF B_Z and other solar wind parameters in our data set, its lagged correlation with *AE* should not be biased by the solar wind structuring. The 35 min delayed correlation between B_Z and *AE* is slightly shorter than the average duration of a substorm growth phase as estimated by Li et al., 2013 from the analysis of 379 events (70 min) and Juusola et al., 2011 from the analysis of 4193 events (72 min), as well as by several other studies based on a lower number of events (e.g., Caan et al., 1977; Foster et al., 1971; Iijima & Nagata, 1972; Iyemori, 1980). However, the time lag for the maximum correlation between *AE* and IMF B_Z is not a direct measurement of the duration of the substorm expansion phase. For instance, Foster et al. (1971) found a substorm growth phase duration of ~80 min on average, while the maximum deviation of *AE* occurred on average 40 min after IMF B_Z reaches its minimum value. Juusola et al. (2011) found the maximum deviation of *AE* occurring ~50 min after the IMF *Bz* minimum. Similarly, Li et al. (2013) defined the substorm growth phase duration as the time interval between IMF southward turning and a strong (100 nT) dropoff of the *AL* index. As shown in their study, the $AU = AE + AL$ index increase precedes the *AL* decrease suggesting that the *AE* increase may occur before the substorm onset as defined by Li et al. (2013). Kamide and Kokubun (1996) analyzed 20 intense isolated substorms and found a growth phase duration of 40 min, in agreement with our results. Li et al. (2013) reported shorter growth phase duration for intense substorms. It is thus also possible that large substorms associated with a large amplitude fluctuation of the *AE* index skew our statistics and shift the highest correlation between B_Z and *AE* toward shorter delays.

We also showed that the solar wind pressure has a direct, quick, and simultaneous effect on the *AE* and *PC* indices. This confirms previous observations indicating that a sudden compression can rapidly increase the energy density in the magnetosphere and trigger geomagnetic activity (e.g., Keika et al., 2009; Lyons et al., 2008). This can also explain why the *AE* and *PC* variations can be simultaneous (when their variation is triggered by the solar wind pressure) or delayed (when triggered by B_Z southward turning) as observed, for instance, by Troshichev and Lukianova (2002).

3.3.2. Correlation Between Solar Wind Parameters and the *SYM-H* Index

Figure 7 shows the correlation coefficient between the *SYM-H* index and solar wind parameters in the same format as Figures 5 and 6.

3.3.2.1. Correlation With IMF Magnitude

The highest correlation coefficient is found for the solar wind magnetic field magnitude B_{SW}. It peaks at a value of $C_{B/SYM\text{-}H} = -0.48$ at $\Delta t = 455$ min (~7.5 h). Similarly to the *PC* and *AE* indices, the peak of the correlation with B_{SW} is asymmetric. While for $\Delta t < 0$ its decrease rate is relatively steep and in agreement with the *SYM-H* and B_{SW} autocorrelation times, it displays a much lower decrease rate for increasing $\Delta t > 0$. $C_{B/SYM\text{-}H}$ is statistically significant up to $\Delta t \sim 5$ days. The long time lag of ~7.5 h is not surprising, since it

indeed takes a while for a solar wind disturbance to propagate into the inner magnetosphere where it affects the ring current and thus *SYM-H*. The fact that the high correlation lasts for a long time is due to the long life time of a ring current enhancement, as already evidenced from the long *SYM-H* autocorrelation time in Figure 1.

3.3.2.2. Correlation With IMF *Bz*

Concerning the IMF components, only B_Z is significantly correlated to *SYM-H*, with a maximum correlation of $C_{Bz/SYM\text{-}H} = 0.37$ at $\Delta t = 80$ min. This time lag is in good agreement with the fact that the beginning of a geomagnetic storm's growth phase (recovery phase) occurs typically 1 to 2 h after a southward (northward) turning of the IMF (e.g., Yermolaev et al., 2010).

Contrary to what was observed for the *PC* and *AE* indices, the shape of the peak of $C_{Bz/SYM\text{-}H}$ is asymmetric. The correlation decreases faster than that of B_{SW}, and $C_{Bz/SYM\text{-}H}$ is statistically significant up to $\Delta t \sim 1$ day. For $\Delta t < 0$, the half width at half height of $C_{Bz/SYM\text{-}H}$ is ~3 h, while for $\Delta t > 0$ it is ~10 h. This is consistent with the fact that large *SYM-H* variations, associated with intense magnetic storms, preferentially occur after long periods (several hours) of southward IMF (e.g., Echer et al., 2008; Gonzalez & Tsurutani, 1987; Yokoyama & Kamide, 1997).

Another difference between *SYM-H* and the *AE* and *PC* indices is that the magnitude of the correlation coefficient for B_{SW} is higher than the one for B_Z. This demonstrates that a southward orientation of the IMF, while it is an important condition for triggering geomagnetic storms, may not be sufficient condition but that also a sufficiently large B_Z value is required for triggering a geomagnetic storm (Gonzalez et al., 1994; Gonzalez & Tsurutani, 1987).

3.3.2.3. Correlation With Solar Wind Velocity, Density, and Pressure

The *SYM-H* index is also correlated to the solar wind velocity ($C_{V/SYM\text{-}H} = -0.42$ at $\Delta t = 135$ min) and to the solar wind pressure ($C_{P/SYM\text{-}H} = -0.31$ at $\Delta t = 725$ min). The solar wind density also displays a significant correlation peak with a maximum correlation coefficient of $C_{N/SYM\text{-}H} = 0.23$ for a negative time lag ($\Delta t = -510$ min). The maximum $C_{N/SYM\text{-}H}$ at -510 min corresponds to a response in the solar wind density ~ 8.5 h after variations in *SYM-H*, which is in contradiction with the causality principle. Instead, it indicates that this correlation mostly results from the solar wind structuring rather than from a direct impact of *SYM-H* on the solar wind density.

3.3.2.4. Conclusions (Correlation Between Solar Wind Parameters and the *SYM-H* Index)

The succession of the peaks of the correlation coefficient of P_{SW}, B_{SW}, V_{SW}, and N_{SW} with *SYM-H* can be compared with the solar wind structuring. The maximum $C_{P/SYM\text{-}H}$ precedes the maximum $C_{B/SYM\text{-}H}$ by 270 min (~4.5 h), of $C_{V/SYM\text{-}H}$ by 590 min (~10 h), and of $C_{N/SYM\text{-}H}$ by 1235 min (~20 h). We can compare it to the delays expected from the solar wind structuring. When V_{SW} is taken as a reference (Figure 3), the maximum correlation for P_{SW} and B_{SW} should occur for approximately the same Δt, and both should precede the maximum correlation of V_{SW} by ~1585 min (26 h) and of N_{SW} by ~2600 min (~43 h). If B_{SW} is taken as a reference (Figure 4), the maximum correlation for P_{SW} should precede the maximum correlation of B_{SW} by 105 min (1.5 h), of V_{SW} by 1645 min (~27.5 h), and of N_{SW} by 2855 min (47.5 h). While the ordering of the correlation maxima between solar wind parameters and *SYM-H* is in agreement with the solar wind structuring, the time lags between the peaks of the correlation differ. This may suggest that solar wind structuring alone cannot account for the observed correlation between solar wind parameters and *SYM-H* and that several solar wind parameters may have a direct effect on the variations of *SYM-H*. However, this may also be due to more complex solar wind structures that cannot be evidenced with such correlation analysis which can only reveal the main solar wind structure. This complexity is reflected in geomagnetic storms which must be seen as extended and complex processes. This has been shown, for instance, for storms driven by magnetic clouds, a subset of CMEs with well-defined magnetic properties (enhanced IMF magnitude and smooth rotation of one IMF component). While most of the storms caused by magnetic clouds are driven by the sheath leading the magnetic cloud region, some can be driven by southward IMF inside the cloud itself (e.g., Wu & Lepping, 2002) which induces several response delays between the IMF B_Z peak value and the minimum *SYM-H* (Gopalswamy, 2008). Another example of the complexity of geomagnetic storms is the two-phase storms, with two dips of the *SYM-H* index. They are relatively common (they represented 25% of the magnetic cloud induced storms studied by Wu & Lepping, 2002) and are likely caused by two portions of southward IMF in magnetic cloud.

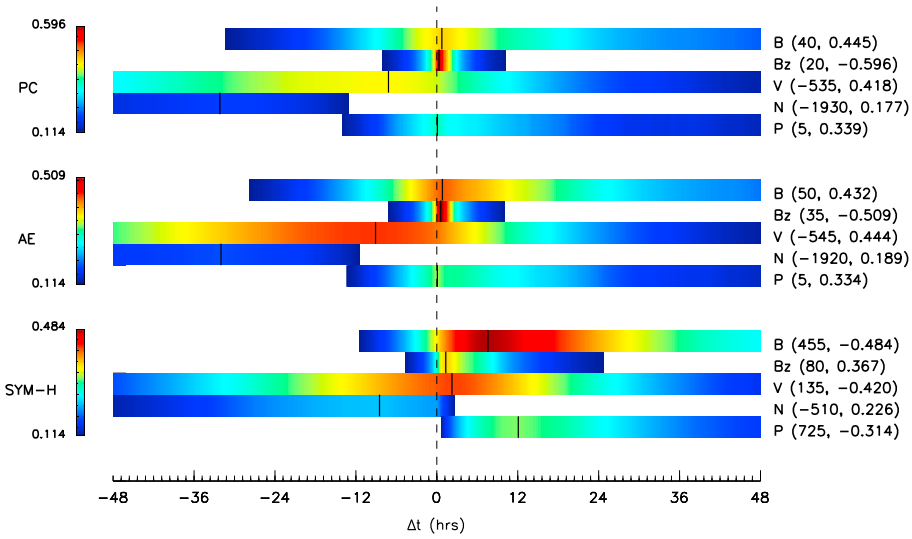

Figure 8. Summary plot of the variation of the absolute value of the correlation coefficient with the time lag for the three indices, *PC*, *AE*, and *SYM-H*. Only solar wind parameters with correlation coefficients higher than the significance threshold are shown. The black vertical lines indicate the corresponding time lag (in minutes) and the maximum of the correlation coefficient the values of which are also indicated in the figure.

4. Summary and Discussion

We have investigated the time response of geomagnetic activity to solar wind and IMF variations by analyzing the lagged cross correlation of solar wind parameters with geomagnetic indices for a period of 11 years. We showed that the structuring of the solar wind as well as the autocorrelation of the solar wind parameters and geomagnetic indices have a strong impact on the results of the correlation analysis.

The strong correlation among the solar wind parameters evidences that they cannot be considered as independent. We showed that the variation of the solar wind cross-correlation coefficients with time lag are globally consistent with the solar wind structures associated with large-scale solar wind transients like CMEs and high-speed solar wind streams and the compression fronts ahead of them.

CMEs, CIRs, and high-speed solar wind streams are associated with large variations of the solar wind parameters from their nominal values. Consequently, even if they represent a small fraction of the analyzed time period, they have a strong impact on the result of the lagged correlation analysis. Similarly, the geomagnetic indices analyzed in this study (*PC*, *AE*, and *SYM-H*) exhibit the most prominent deviations from their standard values during geomagnetically active periods. Their correlation with solar wind parameters thus mostly results from such active periods. As CMEs and CIRs are the most geo-effective solar wind transients, the lagged correlation between solar wind parameters and geomagnetic indices is strongly affected by the solar wind parameters' intercorrelation. It is thus necessary to take this into account when interpreting the correlation between geomagnetic indices and solar wind parameters.

We analyzed the lagged correlation between a set of solar wind parameters and three geomagnetic indices. The values of the maximum correlation and the corresponding time lags are summarized in Figure 8.

Considering the impact of solar wind structuring, our main findings can be summarized as follows:

1. There is no significant correlation between IMF B_X and B_Y components with the *PC*, *AE*, and *SYM-H* indices whatever the time lag.
2. The *PC* and *AE* indices correlate best with IMF B_Z for a time lag of respectively 20 and 35 min, in agreement with the expected lag between these two indices. The correlation peak of IMF B_Z with the *PC* and *AE* indices is sharp in time, indicative of a quick response to IMF B_Z southward turnings.
3. The *PC* and *AE* indices are also well correlated with the solar wind dynamic pressure. They both have a peak correlation for a short time lag (5 min) suggesting that magnetospheric compression by solar wind dynamic pressure can destabilize the magnetotail and rapidly trigger substorm activity.

4. The different timings of the *PC* and *AE* index responses to solar wind dynamic pressure and IMF B_Z can explain observations showing that the *PC* and *AE* variations can be simultaneous or delayed.
5. *SYM-H* is also well correlated with IMF B_Z, while it has an even stronger anticorrelation to the IMF magnitude. The peak correlation between IMF B_Z and *SYM-H* is extended in time. This confirms that intense and long periods of southward IMF (typically a few hours) are required for triggering large geomagnetic storms but also matches the long *SYM-H* autocorrelation time.

While the geomagnetic indices are also well correlated with the other solar wind parameters considered in this study (the solar wind dynamic pressure, velocity, density, and magnetic field magnitude), with correlation coefficients statistically significant for time lags up to days, it is not possible within the scope of the present study to differentiate between a causal effect of these parameters on geomagnetic activity and the role of solar wind structuring. Indeed, if a solar wind parameter appears to be correlated with a geomagnetic index, one should not immediately conclude that this parameter triggers geomagnetic activity. This solar wind parameter may have no causal relation with geomagnetic activity, and the observed correlation may only result from its correlation with other solar wind parameters that do drive geomagnetic activity.

For instance, it has been shown that substorms occur more often during high-speed stream periods (e.g., Slavin et al., 1986; Tanskanen et al., 2005). However, this does not imply that solar wind speed is directly driving substorm occurrences. Indeed, we have shown that solar wind speed is actually correlated with *AE* index but that this correlation is best between *AE* and the solar wind speed as measured several hours after *AE*, in contradiction with the causality principle. This means that statistically the most geo-effective regime of solar wind is the compression region located ahead of high-speed stream regions and not the high-speed stream region itself. This is obviously a statistical consideration and does not mean that solar wind speed does not drive geomagnetic activity. Indeed, it is well known that energy transfer from the solar wind to the magnetosphere is enhanced when solar wind velocity is high. However, storms and substorms are complex phenomena, the occurrence of which depends on magnetospheric preconditioning and on a combination of solar wind parameters which may be statistically more favorable in the compression region ahead of high-speed stream regions.

The interpretation of the correlation between composite solar wind-magnetosphere coupling functions (such as the Akasofu's epsilon parameter, Akasofu, 1981) and geomagnetic indices must similarly take into account the solar wind structuring and the magnetospheric delayed response time. The correlation of such functions with geomagnetic indices may, at least partly, result from the cross correlation between solar wind parameters and does not necessarily prove that this function or what it represents (e.g., the solar wind kinetic energy, the merging electric field, etc.) has actually a direct causal relation with specific aspects of geomagnetic activity.

Correlation analysis is based on mathematical hypotheses that are often not satisfied in the field of space physics. Nonnormal distributions, outliers, a mixture of different regimes, measurement errors, a lack of statistical independence between observations for any parameter or index, and a lack of independence among solar wind parameters may all have a strong impact on the results of a correlation analysis between solar wind parameters and geomagnetic indices. However, while such concerns were raised already in the early age of space physics by Hirshberg and Colburn (1969), they are unfortunately often not taken into account. This is likely to result in biased correlation coefficient estimates or significances, which may lead to misinterpretations. We have attempted to address some of the concerns raised above in the analysis presented here, with the ultimate validation being a consistent physical interpretation of the various correlation factors and time lags. This study demonstrates the need to use more sophisticated methods to study the connection between the parameters of the solar wind and geomagnetic activity. To our knowledge, this is the first study investigating in detail the delayed correlation between solar wind and IMF parameters. We thus did not focus on any specific time period but rather decided to consider a full 11 year time period. Indeed, there was no reason to discard some data to identify the dominant features of the delayed response of geomagnetic activity to solar wind. However, the method developed in this paper could be used in future studies focusing on more specific events, this time with a subset of data. This could enable a more precise identification of the response time for specific categories of event and a comparison of the timescales involved for peculiar geomagnetic or solar wind conditions.

Acknowledgments
We acknowledge use of NASA/GSFC's Space Physics Data Facility's OMNIWeb (or CDAWeb or ftp) service, and OMNI data. R. M., G. C., H. G., L. M., and J. D. K. acknowledge the support by the Belgian Science Policy Office through the Interuniversitary Attraction Pole TOPERS and the Belgian Solar-Terrestrial Centre of Excellence, as well as by the Fonds de la Recherche Scientifique grant PDR T.1073.14 "Comparative study of atmospheric erosion."

References

Aikio, A. T., Pitkänen, T., Honkonen, I., Palmroth, M., & Amm, O. (2013). IMF effect on the polar cap contraction and expansion during a period of substorms. *Annales de Geophysique*, *31*, 1021–1034. https://doi.org/10.5194/angeo-31-1021-2013

Akasofu, S.-I. (1981). Energy coupling between the solar wind and the magnetosphere. *Space Science Reviews*, *28*, 121–191.

Anscombe, F. J. (1971). Graphs in statistical analysis, Published by: Taylor & Francis Ltd. on behalf of the American Statistical Association. *The American Statistician*, *27*, 17–21. https://doi.org/10.2307/2682899

Arnoldy, R. L. (1971). Signature in the interplanetary medium for substorms. *Journal of Geophysical Research*, *76*, 5189–5201. https://doi.org/10.1029/JA076i022p05189

Baker, D. N., Hones, E. W. Jr., Payne, J. B., & Feldman, W. C. (1981). A high time resolution study of interplanetary parameter correlations with *AE*. *Geophysical Research Letters*, *8*, 179–182. https://doi.org/10.1029/GL008i002p00179

Balikhin, M. A., Boynton, R. J., Walker, S. N., Borovsky, J. E., Billings, S. A., & Wei, H. L. (2011). Using the NARMAX approach to model the evolution of energetic electrons fluxes at geostationary orbit. *Geophysical Research Letters*, *38*, L18105. https://doi.org/10.1029/2011GL048980

Bargatze, L. F., Baker, D. N., Hones, E. W. Jr., & McPherron, R. L. (1985). Magnetospheric impulse response for many levels of geomagnetic activity. *Journal of Geophysical Research*, *90*, 6387–6394. https://doi.org/10.1029/JA090iA07p06387

Bargatze, L. F., Ogino, T., McPherron, R. L., & Walker, R. J. (1999). Solar wind magnetic field control of magnetospheric response delay and expansion phase onset timing. *Journal of Geophysical Research*, *104*, 14,583–14,600. https://doi.org/10.1029/1999JA900013

Borovsky, J. E., & Denton, M. H. (2006). Differences between CME-driven storms and CIR-driven storms. *Journal of Geophysical Research*, *111*, A07S08. https://doi.org/10.1029/2005JA011447

Borovsky, J. E., & Denton, M. H. (2010). Solar-wind turbulence and shear: A superposed-epoch analysis of corotating interaction regions at 1 AU. *Journal of Geophysical Research*, *115*, A10101. https://doi.org/10.1029/2009JA014966

Borovsky, J. E., Thomsen, M. F., & Elphic, R. C. (1998). The driving of the plasma sheet by the solar wind. *Journal of Geophysical Research*, *103*, 17,617–17,640. https://doi.org/10.1029/97JA02986

Boudouridis, A., Lyons, L. R., Zesta, E., Weygand, J. M., Ribeiro, A. J., & Ruohoniemi, J. M. (2011). Statistical study of the effect of solar wind dynamic pressure fronts on the dayside and nightside ionospheric convection. *Journal of Geophysical Research*, *116*, A10233. https://doi.org/10.1029/2011JA016582

Boynton, R. J., Balikhin, M. A., Billings, S. A., Wei, H. L., & Ganushkina, N. (2011). Using the NARMAX OLS-ERR algorithm to obtain the most influential coupling functions that affect the evolution of the magnetosphere. *Journal of Geophysical Research*, *116*, A05218. https://doi.org/10.1029/2010JA015505

Brittnacher, M., Wilber, M., Fillingim, M., Chua, D., Parks, G., Spann, J., & Germany, G. (2000). Global auroral response to a solar wind pressure pulse. *Advances in Space Research*, *25*, 1377–1385. https://doi.org/10.1016/S0273-1177(99)00647-X

Browett, S. D., Fear, R. C., Grocott, A., & Milan, S. E. (2016). Timescales for the penetration of IMF B_y into the Earth's magnetotail. *Journal of Geophysical Research: Space Physics*, *122*, 579–593. https://doi.org/10.1002/2016JA023198

Brueckner, G. E. (1974). The behaviour of the outer solar corona (3 *Ro* to 10 *Ro*) during a large solar flare observed from OSO-7 in white light. In G. Newkirk (Ed.), *Coronal Disturbances* (pp. 333–334). Paris: International Astronomical Union.

Caan, M. N., Mcpherron, R. L., & Russell, C. T. (1977). Characteristics of the association between the interplanetary magnetic field and substorms. *Journal of Geophysical Research*, *82*, 4837–4842. https://doi.org/10.1029/JA082i029p04837

Cane, H. V., & Richardson, I. G. (2003). Interplanetary coronal mass ejections in the near-Earth solar wind during 1996–2002, *Journal of Geophysical Research*, *108*(A4), 1156. https://doi.org/10.1029/2002JA009817

Chu, X., McPherron, R. L., Hsu, T.-S., & Angelopoulos, V. (2015). Solar cycle dependence of substorm occurrence and duration: Implications for onset. *Journal of Geophysical Research: Space Physics*, *120*, 2808–2818. https://doi.org/10.1002/2015JA021104

Clauer, C. R., McPherron, R. L., Searls, C., & Kivelson, M. G. (1981). Solar wind control of auroral zone geomagnetic activity. *Geophysical Research Letters*, *8*, 915–918. https://doi.org/10.1029/GL008i008p00915

Daglis, I. A., Thorne, R. M., Baumjohann, W., & Orsini, S. (1999). The terrestrial ring current: Origin, formation, and decay. *Reviews of Geophysics*, *37*, 407–438. https://doi.org/10.1029/1999RG900009

Davis, T. N., & Sugiura, M. (1966). Auroral electrojet activity index *AE* and its universal time variations. *Journal of Geophysical Research*, *71*, 785–801. https://doi.org/10.1029/JZ071i003p00785

Denton, M. H., Borovsky, J. E., Skoug, R. M., Thomsen, M. F., Lavraud, B., Henderson, M. G., … Liemohn, M. W. (2006). Geomagnetic storms driven by ICME- and CIR-dominated solar wind. *Journal of Geophysical Research*, *111*, A07S07. https://doi.org/10.1029/2005JA011436

Dungey, J. W. (1961). Interplanetary magnetic field and the auroral zones. *Physical Review Letters*, *6*, 47–48. https://doi.org/10.1103/PhysRevLett.6.47

Ebihara, Y., & Ejiri, M. (2000). Simulation study on fundamental properties of the storm-time ring current. *Journal of Geophysical Research*, *105*, 15,843–15,860. https://doi.org/10.1029/1999JA900493

Echer, E., Gonzalez, W. D., Tsurutani, B. T., & Gonzalez, A. L. C. (2008). Interplanetary conditions causing intense geomagnetic storms ($Dst \leq -100$ nT) during solar cycle 23 (1996–2006). *Journal of Geophysical Research*, *113*, A05221. https://doi.org/10.1029/2007JA012744

Edgell, S., & Noon, S. (1984). Effect of violation of normality on the *t* test of the correlation coefficient. *Psychological Bulletin*, *95*, 576–583. https://doi.org/10.1037/0033-2909.95.3.576

Eriksson, S., Ergun, R. E., Carlson, C. W., & Peria, W. (2000). The cross-polar potential drop and its correlation to the solar wind. *Journal of Geophysical Research*, *105*, 18,639–18,653. https://doi.org/10.1029/2000JA900033

Fear, R. C., & Milan, S. E. (2012). The IMF dependence of the local time of transpolar arcs: Implications for formation mechanism. *Journal of Geophysical Research*, *117*, A03213. https://doi.org/10.1029/2011JA017209

Forsyth, R. J., & Marsch, E. (1999). Solar origin and interplanetary evolution of stream interfaces. *Space Science Reviews*, *89*, 7.

Foster, J. C., Fairfield, D. H., Ogilvie, K. W., & Rosenberg, T. J. (1971). Relationship of interplanetary parameters and occurrence of magnetospheric substorms. *Journal of Geophysical Research*, *76*(28), 6971–6975. https://doi.org/10.1029/JA076i028p06971

Fuselier, S. A., Trattner, K. J., & Petrinec, S. M. (2000). Cusp observations of high- and low-latitude reconnection for northward interplanetary magnetic field. *Journal of Geophysical Research*, *105*(A1), 253–266. https://doi.org/10.1029/1999JA900422

Gjerloev, J. W., Hoffman, R. A., Friel, M. M., Frank, L. A., & Sigwarth, J. B. (2004). Substorm behavior of the auroral electrojet indices. *Annales de Geophysique*, *22*, 2135–2149. https://doi.org/10.5194/angeo-22-2135-2004

Gonzalez, W. D., Joselyn, J. A., Kamide, Y., Kroehl, H. W., Rostoker, G., Tsurutani, B. T., & Vasyliunas, V. M. (1994). What is a geomagnetic storm? *Journal of Geophysical Research*, *99*(A4), 5771–5792. https://doi.org/10.1029/93JA02867

Gonzalez, W. D., & Tsurutani, B. T. (1987). Criteria of interplanetary parameters causing intense magnetic storms (*Dst* of less than −100 nT). *Planetary and Space Science*, *35*, 1101–1109. https://doi.org/10.1016/0032-0633(87)90015-8

Gonzalez, W. D., Tsurutani, B. T., & Clua de Gonzalez, A. L. (1999). Interplanetary origin of magnetic storms. *Space Science Reviews*, *88*, 529.
Gopalswamy, N. (2008). Solar connections of geoeffective magnetic structures. *Journal of Atmospheric and Solar-Terrestrial Physics*, *70*, 7028. https://doi.org/10.1016/j.jastp.2008.06.010
Gosling, J. T., Hildner, E., MacQueen, R. M., Munro, R. H., Poland, A. I., & Ross, C. L. (1974). Mass ejections from the Sun: A view from Skylab. *Journal of Geophysical Research*, *79*, 4581–4587. https://doi.org/10.1029/JA079i031p04581
Gunell, H., Nilsson, H., Stenberg, G., Hamrin, M., Karlsson, T., Maggiolo, R., … Dandouras, I. (2012). Plasma penetration of the dayside magnetopause. *Physics of Plasmas*, *19*(7), 072906. https://doi.org/10.1063/1.4739446
Haerendel, G. (2011). Six auroral generators: A review. *Journal of Geophysical Research*, *116*, A00K05. https://doi.org/10.1029/2010JA016425
Hairston, M. R., & Heelis, R. A. (1995). Response time of the polar ionospheric convection pattern to changes in the north-south direction of the IMF. *Geophysical Research Letters*, *22*, 631–634. https://doi.org/10.1029/94GL03385
Hasegawa, H., Fujimoto, M., Fujimoto, M., Phan, T.-D., Rème, H., Balogh, A., … TanDokoro, R. (2004). Transport of solar wind into Earth's magnetosphere through rolled-up Kelvin–Helmholtz vortices. *Nature*, *430*, 755–758. https://doi.org/10.1038/nature02799
Hirshberg, J., & Colburn, D. S. (1969). Interplanetary field and geomagnetic variations—A unified view. *Planetary and Space Science*, *17*, 1183–1206. https://doi.org/10.1016/0032-0633(69)90010-5
Hubert, B., Palmroth, M., Laitinen, T. V., Janhunen, P., Milan, S. E., Grocott, A., … Gérard, J.-C. (2006). Compression of the Earth's magnetotail by interplanetary shocks directly drives transient magnetic flux closure. *Geophysical Research Letters*, *33*, L10105. https://doi.org/10.1029/2006GL026008
Hutchinson, J. A., Wright, D. M., & Milan, S. E. (2011). Geomagnetic storms over the last solar cycle: A superposed epoch analysis. *Journal of Geophysical Research*, *116*, A09211. https://doi.org/10.1029/2011JA016463
Iijima, T., & Nagata, T. (1972). Signatures for substorm development of the growth and expansion phase. *Planetary and Space Science*, *20*, 1095.
Iyemori, T. (1980). Time delay of the substorm onset from the IMF southward turning. *Journal of Geomagnetism and Geoelectricity*, *32*, 267–273. https://doi.org/10.5636/jgg.32.267
Jian, L. K., Russell, C., Luhmann, J. G., & Skoug, R. M. (2006). Properties of interplanetary coronal mass ejections at one AU during 1995–2004. *Solar Physics*, *239*, 393–436.
Juusola, L., Østgaard, N., Tanskanen, E., Partamies, N., & Snekvik, K. (2011). Earthward plasma sheet flows during substorm phases. *Journal of Geophysical Research*, *116*, A10228. https://doi.org/10.1029/2011JA016852
Kamide, Y., & Kokubun, S. (1996). Two-component auroral electrojet: Importance for substorm studies. *Journal of Geophysical Research*, *101*(A6), 13,027–13,046. https://doi.org/10.1029/96JA00142
Kane, R. P. (1972). Relationship between the various indices of geomagnetic activity and the interplanetary plasma parameters. *Journal of Atmospheric and Terrestrial Physics*, *34*, 1941–1943.
Kane, R. P. (1974). Relationship between interplanetary plasma parameters and geomagnetic *Dst*. *Journal of Geophysical Research*, *79*, 64–72. https://doi.org/10.1029/JA079i001p00064
Keesee, A. M., Elfritz, J. G., Fok, M.-C., McComas, D. J., & Scime, E. E. (2013). Superposed epoch analyses of ion temperatures during CME- and CIR/HSS-driven storms. *Journal of Atmospheric and Solar-Terrestrial Physics*, *115*, 67–78. https://doi.org/10.1016/j.jastp.2013.08.009
Keika, K., Nakamura, R., Baumjohann, W., Magnes, W., Glassmeier, K. H., Auster, H. U., … Dandouras, I. (2009). Substorm expansion triggered by a sudden impulse front propagating from the dayside magnetopause. *Journal of Geophysical Research*, *114*, A00C24. https://doi.org/10.1029/2008JA013445
Keiling, A., & Takahashi, K. (2011). Review of Pi2 models. *Space Science Reviews*, *161*, 63–148. https://doi.org/10.1007/s11214-011-9818-4
Khan, H., & Cowley, S. W. H. (1999). Observations of the response time of high-latitude ionospheric convection to variations in the interplanetary magnetic field using EISCAT and IMP-8 data. *Annales de Geophysique*, *17*, 1306–1335. https://doi.org/10.1007/s00585-999-1306-8
Koskinen, H. E. J., & Tanskanen, E. I. (2002). Magnetospheric energy budget and the epsilon parameter. *Journal of Geophysical Research*, *107*(A11), 1415. https://doi.org/10.1029/2002JA009283
Kremser, G., & Lundin, R. (1990). Average spatial distributions of energetic particles in the midaltitude cusp/cleft region observed by Viking. *Journal of Geophysical Research*, *95*, 5753–5766. https://doi.org/10.1029/JA095iA05p05753
Li, H., Wang, C., & Kan, J. R. (2011). Contribution of the partial ring current to the *SYM-H* index during magnetic storms. *Journal of Geophysical Research*, *116*, A11222. https://doi.org/10.1029/2011JA016886
Li, H., Wang, C., & Peng, Z. (2013). Solar wind impacts on growth phase duration and substorm intensity: A statistical approach. *Journal of Geophysical Research: Space Physics*, *118*, 4270–4278. https://doi.org/10.1002/jgra.50399
Lindsay, G. M., Luhmann, J. G., Russell, C. T., & Gosling, J. T. (1999). Relationships between coronal mass ejection speeds from coronagraph images and interplanetary characteristics of associated interplanetary coronal mass ejections. *Journal of Geophysical Research*, *104*(A6), 12,515–12,523. https://doi.org/10.1029/1999JA900051
Liou, K., Wu, C.-C., Dryer, M., Wu, S.-T., Rich, N., Plunkett, S., … Schenk, K. (2014). Global simulation of extremely fast coronal mass ejection on 23 July 2012. *Journal of Atmospheric and Solar-Terrestrial Physics*, *121*, 32–41. https://doi.org/10.1016/j.jastp.2014.09.13
Lyons, L. R., Lee, D.-Y., Zou, S., Wang, C.-P., Kozyra, J. U., Weygand, J. M., & Mende, S. B. (2008). Dynamic pressure enhancements as a cause of large-scale stormtime substorms. *Journal of Geophysical Research*, *113*, A08215. https://doi.org/10.1029/2007JA012926
MacQueen, R. M., Eddy, J. A., Gosling, J. T., Hildner, E., Munro, R. H., Newkirk, G. A. Jr., … Ross, C. L. (1974). The outer corona as observed from Skylab: Preliminary results. *The Astrophysical Journal*, *187*, L85–L88.
Mailyan, B., Munteanu, C., & Haaland, S. (2008). What is the best method to calculate the solar wind propagation delay? *Annales de Geophysique*, *26*, 2383–2394. https://doi.org/10.5194/angeo-26-2383-2008
McComas, D. J., Barraclough, B. L., Funsten, H. O., Gosling, J. T., Santiago-Muñoz, E., Skoug, R. M., … Balogh, A. (2000). Solar wind observations over Ulysses' first full polar orbit. *Journal of Geophysical Research*, *105*, 10,419–10,433. https://doi.org/10.1029/1999JA000383
Meng, C.-I., Tsurutani, B., Kawasaki, K., & Akasofu, S.-I. (1973). Cross-correlation analysis of the *AE* index and the interplanetary magnetic field B_z component. *Journal of Geophysical Research*, *78*, 617–629. https://doi.org/10.1029/JA078i004p00617
Nagata, D., Machida, S., Ohtani, S., Saito, Y., & Mukai, T. (2008). Solar wind control of plasma number density in the near-Earth plasma sheet: Three-dimensional structure. *Annales Geophysicae*, *26*, 4031–4049. https://doi.org/10.5194/angeo-26-4031-2008
Nakamura, R. (2006). Substorms and their solar wind causes. *Space Science Reviews*, *124*, 91–101. https://doi.org/10.1007/s11214-006-9131-9
Nakamura, R., Bargatze, L. F., Mukai, T., Nagai, T., Baker, K. B., Hairston, M. R., … Troshichev, O. A. (1999). Response of the midtail electric field to enhanced solar wind energy input. *Journal of Geophysical Research*, *104*, 17,299–17,310. https://doi.org/10.1029/1999JA900166

Newell, P. T., & Liou, K. (2011). Solar wind driving and substorm triggering. *Journal of Geophysical Research*, *116*, A03229. https://doi.org/10.1029/2010JA016139

Newell, P. T., Sotirelis, T., Liou, K., Meng, C.-I., & Rich, F. J. (2007). A nearly universal solar wind-magnetosphere coupling function inferred from 10 magnetospheric state variables. *Journal of Geophysical Research*, *112*, A01206. https://doi.org/10.1029/2006JA012015

Paschmann, G., Papamastorakis, I., Sckopke, N., Haerendel, G., Sonnerup, B. U. O., Bame, S. J., … Elphic, R. C. (1979). Plasma acceleration at the Earth's magnetopause—Evidence for reconnection. *Nature*, *282*, 243–246. https://doi.org/10.1038/282243a0

Pearson, E. S. (1931). The test of significance for the correlation coefficient. *Journal of the American Statistical Association*, *26*, 128–134.

Pearson, E. S. (1932). The test of significance for the correlation coefficient: Some further results. *Journal of the American Statistical Association*, *27*, 424–426.

Pearson, K. (1920). Notes on the history of correlation. *Biometrika*, *13*, 25–45.

Peat, J., & Barton, B. (2005). Continuous Data Analyses: Correlation and Regression. In *Medical Statistics: A Guide to Data Analysis and Critical Appraisal* (pp. 156–201). Malden, MA: Blackwell Publishing Inc. https://doi.org/10.1002/9780470755945.ch6

Pitkänen, T., Hamrin, M., Kullen, A., Maggiolo, R., Karlsson, T., Nilsson, H., & Norqvist, P. (2016). Response of magnetotail twisting to variations in IMF B_y: A THEMIS case study 1–2 January 2009. *Geophysical Research Letters*, *43*, 7822–7830. https://doi.org/10.1002/2016GL070068

Rostoker, G., Akasofu, S.-I., Foster, J., Greenwald, R., Kamide, Y., Kawasaki, K., … Russell, C. (1980). Magnetospheric substorms—Definition and signatures. *Journal of Geophysical Research*, *85*(A4), 1663–1668. https://doi.org/10.1029/JA085iA04p01663

Rostoker, G., Lam, H.-L., & Hume, W. D. (1972). Response time of the magnetosphere to the interplanetary electric field. *Canadian Journal of Physics*, *50*, 544. https://doi.org/10.1139/p72-073

Russell, C. T. (2001). Solar wind and interplanetary magnetic field: A tutorial. In P. Song, H. J. Singer, & G. L. Siscoe (Eds.), *Space Weather* (pp. 73–89). Washington, DC: American Geophysical Union. https://doi.org/10.1029/GM125p0073

Russell, C. T., & McPherron, R. L. (1973). The magnetotail and substorms. *Space Science Reviews*, *15*, 205–266. https://doi.org/10.1007/BF00169321

Slavin, J. A., Jungman, G., & Smith, E. J. (1986). The interplanetary magnetic field during solar cycle 21 ISEE-3/ICE observations. *Geophysical Research Letters*, *13*, 513. https://doi.org/10.1029/GL013i006p00513

Sugiura, M. (1964). Hourly values of equatorial *Dst* for IGY. In *Annals of the International Geophysical Year* (Vol. 35, pp. 7–45). Oxford: Pergamon Press.

Takalo, J., & Timonen, J. (1998). On the relation of the *AE* and *PC* indices. *Journal of Geophysical Research*, *103*, 29,393–29,398. https://doi.org/10.1029/98JA02390

Tanskanen, E. I., Slavin, J. A., Tanskanen, A. J., Viljanen, A., Pulkkinen, T. I., Koskinen, H. E. J., … Eastwood, J. (2005). Magnetospheric substorms are strongly modulated by interplanetary high-speed streams. *Geophysical Research Letters*, *32*, L16104. https://doi.org/10.1029/2005GL023318

Tenfjord, P., Østgaard, N., Snekvik, K., Laundal, K. M., Reistadt, J. P., Haaland, S., & Milan, S. E. (2015). How the IMF B_y induces a B_y component in the closed magnetosphere and how it leads to asymmetric currents and convection patterns in the two hemispheres. *Journal of Geophysical Research: Space Physics*, *120*, 9368–9384. https://doi.org/10.1002/2015JA021579

Tokumaru, M., Kojima, M., & Fujiki, K. (2010). Solar cycle evolution of the solar wind speed distribution from 1985 to 2008. *Journal of Geophysical Research*, *115*, A04102. https://doi.org/10.1029/2009JA014628

Tousey, R. (1973). The solar corona. *Space Research*, *XIII*, 713–730.

Troshichev, O. A., & Andrezen, V. G. (1985). The relationship between interplanetary quantities and magnetic activity in the southern polar cap. *Planetary and Space Science*, *33*, 415–419. https://doi.org/10.1016/0032-0633(85)90086-8

Troshichev, O. A., Andrezen, V. G., Vennerstrøm, S., & Friis-Christensen, E. (1988). Magnetic activity in the polar cap—A new index. *Planetary and Space Science*, *36*, 1095–1102. https://doi.org/10.1016/0032-0633(88)90063-3

Troshichev, O. A., & Lukianova, R. (2002). Relation of the PC index to the solar wind parameters and substorm activity in time of magnetic storm. *Journal of Atmospheric and Solar-Terrestrial Physics*, *64*(5–6), 585–591. https://doi.org/10.1016/S1364-6826(02)00016-0

Tsurutani, B. T., & Thorne, R. M. (1982). Diffusion processes in the magnetopause boundary layer. *Geophysical Research Letters*, *9*, 1247–1250. https://doi.org/10.1029/GL009i011p01247

Vassiliadis, D., Angelopoulos, V., Baker, D. N., & Klimas, A. J. (1996). The relation between the northern polar cap and auroral electrojet geomagnetic indices in the wintertime. *Geophysical Research Letters*, *23*, 2781–2784. https://doi.org/10.1029/96GL02575

Vennerstrøm, S., Friis-Christensen, E., Troshichev, O. A., & Andrezen, V. G. (1991). Comparison between the polar cap index *PC* and the auroral electrojet indices *AE*, *AL* and *AU*. *Journal of Geophysical Research*, *96*(A1), 101–113. https://doi.org/10.1029/90JA01975

Villante, U., Lepidi, S., Francia, P., & Bruno, T. (2004). Some aspects of the interaction of interplanetary shocks with the Earth's magnetosphere: An estimate of the propagation time through the magnetosheath. *Journal of Atmospheric and Solar-Terrestrial Physics*, *66*, 337–341. https://doi.org/10.1016/j.jastp.2004.01.003

Wanliss, J. A., & Showalter, K. M. (2006). High-resolution global storm index: *Dst* versus *SYM-H*. *Journal of Geophysical Research*, *111*, A02202. https://doi.org/10.1029/2005JA011034

Wilcox, J. M., Schatten, K. H., & Ness, N. F. (1967). Influence of interplanetary magnetic field and plasma on geomagnetic activity during quiet-Sun conditions. *Journal of Geophysical Research*, *72*, 19–26. https://doi.org/10.1029/JZ072i001p00019

Wing, S., Johnson, J. R., Camporeale, E., & Reeves, G. D. (2016). Information theoretical approach to discovering solar wind drivers of the outer radiation belt. *Journal of Geophysical Research: Space Physics*, *121*, 9378–9399. https://doi.org/10.1002/2016JA022711

Wu, C.-C., & Lepping, R. P. (2002). Effects of magnetic clouds on the occurrence of geomagnetic storms: The first 4 years of Wind. *Journal of Geophysical Research, 107*(A10), 1314, https://doi.org/10.1029/2001JA000161

Yamada, M., Kulsrud, R., & Ji, H. (2010). Magnetic reconnection. *Reviews of Modern Physics*, *82*, 603–664. https://doi.org/10.1103/RevModPhys.82.603

Yermolaev, Y. I., Nikolaeva, N. S., Lodkina, I. G., & Yermolaev, M. Y. (2010). Specific interplanetary conditions for CIR-, Sheath-, and ICME-induced geomagnetic storms obtained by double superposed epoch analysis. *Annales de Geophysique*, *28*, 2177–2186. https://doi.org/10.5194/angeo-28-2177-2010

Yokoyama, N., & Kamide, Y. (1997). Statistical nature of geomagnetic storms. *Journal of Geophysical Research*, *102*(A7), 14,215–14,222. https://doi.org/10.1029/97JA00903

Zesta, E., Singer, H. J., Lummerzheim, D., Russell, C. T., Lyons, L. R., & Brittnacher, M. J. (2000). The Effect of the January 10, 1997, Pressure Pulse on the Magnetosphere-Ionosphere Current System. In S.-I. Ohtani, et al. (Eds.), *Magnetospheric Current Systems* (pp. 217–226). Washington, DC: American Geophysical Union. https://doi.org/10.1029/GM118p0217